

UNIVERSIDAD DE CONCEPCIÓN



CENTRO DE INVESTIGACIÓN EN  
INGENIERÍA MATEMÁTICA (CI<sup>2</sup>MA)



A posteriori error analysis of mixed finite element methods for  
a regularized  $\mu(I)$ -rheology model of granular materials

SERGIO CAUCAO, GABRIEL N. GATICA,  
SAULO MEDRADO, YURI D. SOBRAL

PREPRINT 2025-09

SERIE DE PRE-PUBLICACIONES



# *A posteriori* error analysis of mixed finite element methods for a regularized $\mu(I)$ -rheology model of granular materials\*

SERGIO CAUCAO<sup>†</sup> GABRIEL N. GATICA<sup>‡</sup> SAULO R. MEDRADO<sup>§</sup> YURI D. SOBRAL<sup>¶</sup>

## Abstract

We consider a Banach spaces-based mixed variational formulation recently proposed for the stationary  $\mu(I)$ -rheology model of granular materials, and develop the first reliable and efficient residual-based *a posteriori* error estimator for its associated mixed finite element scheme in both 2D and 3D, considering PEERS and AFW-based discretizations. For the reliability analysis, and due to the nonlinear nature of the problem, we employ the first-order Gâteaux derivative of the global operator involved in the problem, combined with appropriate small-data assumptions, a stable Helmholtz decomposition in nonstandard Banach spaces, and local approximation properties of the Raviart–Thomas and Clément interpolants. In turn, inverse inequalities, the localization technique based on bubble functions in local  $L^p$ -spaces, and known results from previous works are the main tools yielding the efficiency estimate. Finally, several numerical examples confirming the theoretical properties of the estimator and illustrating the performance of the associated adaptive algorithms are reported. In particular, the case of fluid flow through a 2D cavity with two circular obstacles is considered.

**Keywords:** granular flows, nonlinear viscosity, mixed finite elements, Banach spaces, *a posteriori* error analysis, reliability, efficiency.

**Mathematics subject classifications (2000):** 65N30, 65N12, 65N15, 35Q79, 76R05, 76D07

## 1 Introduction

We recently introduced and analyzed in [12] a Banach spaces-based mixed variational formulation for the regularized  $\mu(I)$ -rheology model of granular flows, which is described by a Navier–Stokes-like equation where the equivalent viscosity depends nonlinearly on both the pressure and the Euclidean norm of the symmetric part of the velocity gradient in  $\mathbb{R}^n$ , with  $n \in \{2, 3\}$ . In that work, in addition

---

\*This research was supported by ANID-Chile through the projects CENTRO DE MODELAMIENTO MATEMÁTICO (FB210005) and Fondecyt 1250937; by Grupo de Investigación en Análisis Numérico y Cálculo Científico (GIANuC<sup>2</sup>), Universidad Católica de la Santísima Concepción; by Centro de Investigación en Ingeniería Matemática (CI<sup>2</sup>MA), Universidad de Concepción; and by Fundação de Apoio à Pesquisa do Distrito Federal (FAPDF) project number 00193-00001821/2022-21.

<sup>†</sup>GIANuC<sup>2</sup> and Departamento de Matemática y Física Aplicadas, Universidad Católica de la Santísima Concepción, Casilla 297, Concepción, Chile, email: scaucao@ucsc.cl.

<sup>‡</sup>CI<sup>2</sup>MA and Departamento de Ingeniería Matemática, Universidad de Concepción, Casilla 160-C, Concepción, Chile, email: ggatica@ci2ma.udec.cl.

<sup>§</sup>Departamento de Matemática, Universidade de Brasília, Campus Universitário Darcy Ribeiro, 70910-900 Brasília, DF, Brazil, email: saulo\_medrado@hotmail.com

<sup>¶</sup>Departamento de Matemática, Universidade de Brasília, Campus Universitário Darcy Ribeiro, 70910-900 Brasília, DF, Brazil, email: ydsobral@unb.br.

to the velocity, pressure, and strain rate tensor, a modified stress tensor that includes the convective term, and the skew-symmetric vorticity were introduced as additional unknowns, leading to a nonlinear twofold saddle point-based mixed variational formulation in a Banach space framework. The pressure is determined through an iterative postprocess suggested by the incompressibility condition of the fluid, which allows us to express this unknown in terms of the aforementioned stress and velocity. A fixed-point strategy, combined with a solvability result for a class of nonlinear twofold saddle point operator equations in Banach spaces, is employed to show, along with the classical Banach fixed-point theorem and suitable small data assumptions, the well-posedness of both the continuous and discrete formulations. In particular, PEERS (resp. AFW) elements of order  $\ell \geq 0$  for the stress, velocity, and skew-symmetric vorticity, along with piecewise polynomials of degree  $\leq \ell + n$  (resp.  $\leq \ell + 1$ ) for the strain rate, yield stable Galerkin schemes. Stability, convergence, and optimal *a priori* error estimates were also derived in [12].

It is well known that adaptive algorithms based on *a posteriori* error estimates are particularly effective in recovering the loss of convergence orders often observed in standard Galerkin procedures, such as finite element and mixed finite element methods. This is especially true when these methods are applied to nonlinear problems, where singularities or high gradients in the exact solutions are present. In this context, the study of *a posteriori* error estimators for saddle-point problems has been widely developed in the literature by various authors (see, e.g., [2], [10], [11], [34], [37], and references therein). In particular, this powerful approach has been successfully applied to the Navier–Stokes equations, both with constant and nonlinear viscosity, as well as to related models. We refer to pioneering works such as [35], [40], and [38], as well as to [3, Section 9.3], where the first contributions to derive an *a posteriori* error analysis for the incompressible Navier–Stokes problem in its classical velocity-pressure formulation were introduced. Later, the *a priori* and *a posteriori* error analysis for the dual mixed finite element method of the Navier–Stokes problem were proposed and developed in [23]. Additionally, we mention [4], where the authors extend these contributions to the case of Dirac measures, and [33], which provides an *a posteriori* error analysis for a Discontinuous Galerkin scheme that offers exactly divergence-free approximations of the velocity. Meanwhile, adaptive methods for augmented-mixed formulations for the Navier–Stokes problem with constant and variable viscosity were developed in [30] and [9], respectively. We also refer to [14], where the authors developed an *a posteriori* error analysis for a fully-mixed formulation of the Navier–Stokes/Darcy coupled problem with nonlinear viscosity. In this work, a suitable first-order Gâteaux derivative of the global operator involved is employed to derive the corresponding reliability of the estimator. Furthermore, [8] is particularly notable for its *a posteriori* error analysis of a momentum-conservative Banach spaces-based mixed finite element method for the Navier–Stokes problem. In this work, standard duality-based arguments, a suitable Helmholtz decomposition within Banach frameworks, and classical approximation properties are combined with small data assumptions to establish the reliability of the estimators. Similar techniques have been employed in [18] and [28] to develop reliable and efficient residual-based *a posteriori* error estimators in both 2D and 3D for Banach spaces-based mixed finite element methods applied to the stationary Boussinesq and Oberbeck-Boussinesq systems. Lastly, we refer to [13] for a recent *a posteriori* error analysis of a Banach spaces-based mixed formulation for the coupled Brinkman–Forchheimer and double-diffusion equations.

Building upon the previous discussion and extending the study initiated in [12] on a regularized  $\mu(I)$ -rheology model for granular materials described by a Navier–Stokes-like equation, this paper employs and adapts the *a posteriori* error analysis techniques developed in [14], [8], [28], and [13] for mixed formulations in Hilbert and Banach spaces to the current  $\mu(I)$ -rheology model. We construct a reliable and efficient residual-based *a posteriori* error estimator for the 2D and 3D versions of the mixed finite element methods introduced in [12]. Specifically, we derive a global quantity  $\Theta$  that is

formulated in terms of computable local indicators  $\Theta_K$ , each associated with an element  $K$  of a given triangulation  $\mathcal{T}_h$ . This allows for the identification of error sources and the design of an adaptive meshing algorithm to enhance computational efficiency. In this setting, the estimator  $\Theta$  is considered efficient (resp. reliable) if there exist positive constants  $C_{\text{eff}}$  (resp.  $C_{\text{rel}}$ ), independent of the mesh sizes, such that

$$C_{\text{eff}} \Theta + \text{h.o.t.} \leq \|\text{error}\| \leq C_{\text{rel}} \Theta + \text{h.o.t.},$$

where  $\text{h.o.t.}$  represents one or more higher-order terms. To the best of the authors' knowledge, this work presents the first *a posteriori* error analysis of Banach spaces-based mixed finite element methods for the stationary  $\mu(I)$ -rheology equations governing granular materials.

This paper is organized as follows. The remainder of this section introduces some standard notations and functional spaces. In Section 2, we revisit the model problem from [12] along with its continuous and discrete mixed variational formulations. Next, in Section 3, we provide a detailed derivation of a reliable and efficient residual-based *a posteriori* error estimator for the 2D version of the problem. In particular, the reliability analysis considers a suitable Helmholtz decomposition in a Banach spaces setting, with its discrete version employing PEERS and AFW-based elements. Several numerical results illustrating the reliability and efficiency of the estimator, the effectiveness of the associated adaptive algorithm, and the recovery of optimal convergence rates are reported in Section 4. Finally, additional properties required for the derivation of the reliability and efficiency estimates are provided in Appendices A and B, respectively. In turn, the 3D version of the *a posteriori* error estimator, building upon the results in Section 3, is established in Appendix C.

## Preliminary notations

In what follows,  $\Omega \subset \mathbb{R}^n$ , with  $n \in \{2, 3\}$ , denotes a bounded domain with Lipschitz-continuous boundary  $\Gamma$  and outward unit normal vector  $\boldsymbol{\nu}$ . Then, we adopt the usual notation for Lebesgue spaces  $L^t(\Omega)$  and Sobolev spaces  $W^{l,t}(\Omega)$  and  $W_0^{l,t}(\Omega)$ , with  $l \geq 0$  and  $t \in [1, +\infty)$ , whose corresponding norms, either for the scalar or vectorial case, are denoted by  $\|\cdot\|_{0,t;\Omega}$  and  $\|\cdot\|_{l,t;\Omega}$ , respectively. In particular,  $W^{0,t}(\Omega) = L^t(\Omega)$ , and when  $t = 2$  we write  $H^l(\Omega)$  instead of  $W^{l,2}(\Omega)$ , with the corresponding norm and seminorm denoted by  $\|\cdot\|_{l,\Omega}$  and  $|\cdot|_{l,\Omega}$ , respectively. In addition, given any generic scalar function space  $M$ , we let  $\mathbf{M}$  and  $\mathbb{M}$  be its vectorial and tensorial counterparts, respectively, whereas  $M'$  represents its dual space, whose norm is defined by  $\|f\|_{M'} := \sup_{0 \neq v \in M} \frac{|f(v)|}{\|v\|_M}$ . Also,  $\mathbb{I}$  stands for the identity tensor in  $\mathbb{R}^{n \times n}$ , and, besides denoting the absolute value in  $\mathbb{R}$ ,  $|\cdot|$  stands for the Euclidean norms in  $\mathbb{R}^n$  and  $\mathbb{R}^{n \times n}$ . In turn, for any vector fields  $\mathbf{v} = (v_i)_{i=1,n}$  and  $\mathbf{w} = (w_i)_{i=1,n}$ , we set the gradient, divergence, and tensor product operators, respectively, as

$$\nabla \mathbf{v} := \left( \frac{\partial v_i}{\partial x_j} \right)_{i,j=1,n}, \quad \text{div}(\mathbf{v}) := \sum_{j=1}^n \frac{\partial v_j}{\partial x_j}, \quad \text{and} \quad \mathbf{v} \otimes \mathbf{w} := (v_i w_j)_{i,j=1,n}.$$

On the other hand, for any tensor fields  $\boldsymbol{\tau} = (\tau_{ij})_{i,j=1,n}$  and  $\boldsymbol{\zeta} = (\zeta_{ij})_{i,j=1,n}$ , we let  $\mathbf{div}(\boldsymbol{\tau})$  be the divergence operator  $\text{div}$  acting along the rows of  $\boldsymbol{\tau}$ , and define the transpose, the matrix trace, the tensor inner product operators, and the deviatoric tensor, respectively, as

$$\boldsymbol{\tau}^t = (\tau_{ji})_{i,j=1,n}, \quad \text{tr}(\boldsymbol{\tau}) = \sum_{i=1}^n \tau_{ii}, \quad \boldsymbol{\tau} : \boldsymbol{\zeta} := \sum_{i,j=1}^n \tau_{ij} \zeta_{ij}, \quad \text{and} \quad \boldsymbol{\tau}^d := \boldsymbol{\tau} - \frac{1}{n} \text{tr}(\boldsymbol{\tau}) \mathbb{I}. \quad (1.1)$$

Furthermore, given  $t \in (1, +\infty)$ , we introduce the Banach space

$$\mathbb{H}(\mathbf{div}_t; \Omega) := \left\{ \boldsymbol{\tau} \in \mathbb{L}^2(\Omega) : \mathbf{div}(\boldsymbol{\tau}) \in \mathbf{L}^t(\Omega) \right\}, \quad (1.2)$$

which is endowed with the natural norm defined by

$$\|\boldsymbol{\tau}\|_{\mathbf{div}_t; \Omega} := \|\boldsymbol{\tau}\|_{0, \Omega} + \|\mathbf{div}(\boldsymbol{\tau})\|_{0, t; \Omega} \quad \forall \boldsymbol{\tau} \in \mathbb{H}(\mathbf{div}_t; \Omega).$$

Then, following [24, eq. (1.43), Section 1.3.4], one can easily verify that the following holds for each

$$t \in \begin{cases} (1, +\infty) & \text{if } n = 2 \\ [6/5, +\infty) & \text{if } n = 3 \end{cases},$$

$$\langle \boldsymbol{\tau} \boldsymbol{\nu}, \mathbf{v} \rangle = \int_{\Omega} \left\{ \boldsymbol{\tau} : \nabla \mathbf{v} + \mathbf{v} \cdot \mathbf{div}(\boldsymbol{\tau}) \right\} \quad \forall (\boldsymbol{\tau}, \mathbf{v}) \in \mathbb{H}(\mathbf{div}_t; \Omega) \times \mathbf{H}^1(\Omega), \quad (1.3)$$

where  $\langle \cdot, \cdot \rangle$  stands for the duality pairing between  $\mathbf{H}^{-1/2}(\Gamma)$  and  $\mathbf{H}^{1/2}(\Gamma)$ .

## 2 The mathematical model and its variational formulation

In this section, we recall from [12] the model problem, its mixed variational formulation, and the associated mixed finite element methods.

### 2.1 The $\mu(I)$ -rheology model of granular materials

In what follows, we consider the model analyzed in [12] (see also [32]), which describes the steady-state flow of a granular material based on the  $\mu(I)$ -rheology approach. More precisely, given a source term  $\mathbf{f}$ , we focus on solving an incompressible Navier–Stokes-like equation, which requires determining a velocity field  $\mathbf{u}$  and a pressure field  $p$  such that

$$\begin{aligned} \rho(\nabla \mathbf{u}) \mathbf{u} &= \mathbf{div}(\eta(p, |\mathbf{D}|) \mathbf{D}) - \nabla p + \mathbf{f} \quad \text{in } \Omega, \quad \mathbf{div}(\mathbf{u}) = 0 \quad \text{in } \Omega, \\ \mathbf{u} &= \mathbf{u}_D \quad \text{on } \Gamma, \quad \text{and} \quad \int_{\Omega} p = \kappa, \end{aligned} \quad (2.1)$$

where  $\rho$  denotes the density,  $\mathbf{D} := \frac{1}{2}(\nabla \mathbf{u} + (\nabla \mathbf{u})^\top)$  represents the symmetric part of the velocity gradient, satisfying

$$|\mathbf{D}| = \sqrt{\mathbf{D} : \mathbf{D}} \quad \text{and} \quad \text{tr}(\mathbf{D}) = \mathbf{div}(\mathbf{u}) = 0, \quad (2.2)$$

$\kappa$  is a positive constant, and given  $0 < \varepsilon \ll 1$ ,  $\eta : \mathbb{R}^+ \times \mathbb{R}^+ \rightarrow \mathbb{R}^+$  is a regularized function (see [12, eqs. (2.9)–(2.11) for details]) defined as

$$\eta(\varrho, \omega) := \frac{a_1 \varrho}{\omega + \varepsilon} + \frac{a_2 \varrho}{a_3 \sqrt{\varrho} + a_4 \omega + \varepsilon} \quad \forall (\varrho, \omega) \in \mathbb{R}^+ \times \mathbb{R}^+, \quad (2.3)$$

with positive coefficients  $a_i$ ,  $i \in \{1, 2, 3, 4\}$ , given by

$$a_1 := \sqrt{2} \mu_s, \quad a_2 := 2d(\mu_d - \mu_s), \quad a_3 := \rho^{-1/2} I_0, \quad \text{and} \quad a_4 := \sqrt{2} d,$$

where the coefficients  $\mu_s$  and  $\mu_d$  correspond, respectively, to the static and dynamic friction limits, and  $I_0$  is a positive reference (experimental) constant. Owing to the incompressibility of the fluid, the datum  $\mathbf{u}_D \in \mathbf{H}^{1/2}(\Gamma)$  must satisfy the compatibility condition

$$\int_{\Gamma} \mathbf{u}_D \cdot \boldsymbol{\nu} = 0. \quad (2.4)$$

We observe that the internal friction coefficient of the granular continuum  $\mu$  (cf. [12, eq. (2.7)]) can be computed by using the formula

$$\mu(I) := \mu_s + \left( \frac{\mu_d - \mu_s}{I + I_0} \right) I \quad \text{with} \quad I = \frac{\sqrt{2} d |\mathbf{D}|}{\sqrt{p/\rho}}.$$

Next, in order to derive a mixed formulation for (2.1), in which the Dirichlet boundary condition for the velocity becomes a natural one, we now proceed as in [12, Section 2] and introduce as a further unknown a modified stress tensor  $\boldsymbol{\sigma}$ , which is defined by

$$\boldsymbol{\sigma} := \eta(p, |\mathbf{D}|) \mathbf{D} - p \mathbb{I} - \rho(\mathbf{u} \otimes \mathbf{u}), \quad (2.5)$$

so that recalling that the overall density is constant, and noting that the incompressibility condition allows us to show that  $\mathbf{div}(\mathbf{u} \otimes \mathbf{u}) = (\nabla \mathbf{u}) \mathbf{u}$ , we deduce that the momentum equation can be rewritten as

$$\mathbf{div}(\boldsymbol{\sigma}) + \mathbf{f} = 0 \quad \text{in } \Omega.$$

Moreover, applying deviatoric operator (cf. (1.1)) to (2.5), and using the last equation in (2.2), which obviously yields  $\mathbf{D}^d = \mathbf{D}$ , we find that

$$\boldsymbol{\sigma}^d := \eta(p, |\mathbf{D}|) \mathbf{D} - \rho(\mathbf{u} \otimes \mathbf{u})^d \quad \text{in } \Omega. \quad (2.6)$$

In turn, applying now matrix trace to (2.5), we obtain an explicit formula for the pressure  $p$  in terms of  $\boldsymbol{\sigma}$  and  $\mathbf{u}$ , namely

$$p = -\frac{1}{n} \text{tr}(\boldsymbol{\sigma} + \rho(\mathbf{u} \otimes \mathbf{u})). \quad (2.7)$$

We remark here that (2.5) and the incompressibility condition given by the second equation in (2.1) are jointly equivalent to (2.6)–(2.7). On the other hand, in order to perform the usual integration by parts procedure required by a mixed formulation, which reduces to be able to test  $\nabla \mathbf{u}$ , we now decompose  $\mathbf{D}$  as

$$\mathbf{D} = \nabla \mathbf{u} - \boldsymbol{\gamma}, \quad \text{with} \quad \boldsymbol{\gamma} := \frac{1}{2} \left( \nabla \mathbf{u} - (\nabla \mathbf{u})^\dagger \right),$$

where  $\boldsymbol{\gamma}$  is an auxiliary known whose diagonal entries are all zero, while the off-diagonal ones contain the components of the vorticity  $\nabla \times \mathbf{u}$ . Summarizing, (2.1) can be equivalently reformulated as: Find  $\mathbf{D}$ ,  $\boldsymbol{\sigma}$ ,  $\mathbf{u}$ ,  $\boldsymbol{\gamma}$ , and  $p$  in suitable spaces to be indicated below such that

$$\begin{aligned} \mathbf{D} - \nabla \mathbf{u} + \boldsymbol{\gamma} &= \mathbf{0} \quad \text{in } \Omega, \\ \eta(p, |\mathbf{D}|) \mathbf{D} - \boldsymbol{\sigma}^d - \rho(\mathbf{u} \otimes \mathbf{u})^d &= \mathbf{0} \quad \text{in } \Omega, \\ \mathbf{div}(\boldsymbol{\sigma}) + \mathbf{f} &= \mathbf{0} \quad \text{in } \Omega, \\ p &= -\frac{1}{n} \text{tr}(\boldsymbol{\sigma} + \rho(\mathbf{u} \otimes \mathbf{u})) \quad \text{in } \Omega, \quad \mathbf{u} = \mathbf{u}_D \quad \text{on } \Gamma, \quad \text{and} \quad \int_{\Omega} p = \kappa. \end{aligned} \quad (2.8)$$

## 2.2 The mixed variational formulation

We first recall the following scalar and tensorial functional spaces from [12, Section 3] (cf. (1.2)):

$$L^2_{\kappa}(\Omega) := \left\{ q \in L^2(\Omega) : \int_{\Omega} q = \kappa, \quad \kappa > 0 \right\},$$

$$\begin{aligned}
\mathbb{L}_{\text{tr}}^2(\Omega) &:= \left\{ \mathbf{E} \in \mathbb{L}^2(\Omega) : \text{tr}(\mathbf{E}) = 0 \right\}, \\
\mathbb{L}_{\text{sk}}^2(\Omega) &:= \left\{ \boldsymbol{\xi} \in \mathbb{L}^2(\Omega) : \boldsymbol{\xi}^{\text{t}} = -\boldsymbol{\xi} \right\}, \\
\mathbb{H}_0(\mathbf{div}_{4/3}; \Omega) &:= \left\{ \boldsymbol{\tau} \in \mathbb{H}(\mathbf{div}_{4/3}; \Omega) : \int_{\Omega} \text{tr}(\boldsymbol{\tau}) = 0 \right\},
\end{aligned}$$

and observe that the following decomposition holds:

$$\mathbb{H}(\mathbf{div}_{4/3}; \Omega) = \mathbb{H}_0(\mathbf{div}_{4/3}; \Omega) \oplus \mathbb{R}\mathbb{I}. \quad (2.9)$$

Next, for sake of clarity, we introduce the spaces

$$\mathcal{H}_1 := \mathbb{L}_{\text{tr}}^2(\Omega), \quad \mathcal{H}_2 := \mathbb{H}_0(\mathbf{div}_{4/3}; \Omega), \quad \text{and} \quad \mathcal{Q} := \mathbf{L}^4(\Omega) \times \mathbb{L}_{\text{sk}}^2(\Omega), \quad (2.10)$$

set the notations

$$\vec{\mathbf{u}} := (\mathbf{u}, \gamma), \quad \vec{\mathbf{v}} := (\mathbf{v}, \boldsymbol{\xi}) \in \mathcal{Q},$$

and endow  $\mathcal{H}_1$ ,  $\mathcal{H}_2$ , and  $\mathcal{Q}$ , respectively, with the norms:

$$\|\mathbf{E}\|_{\mathcal{H}_1} := \|\mathbf{E}\|_{0,\Omega}, \quad \|\boldsymbol{\tau}\|_{\mathcal{H}_2} := \|\boldsymbol{\tau}\|_{\mathbf{div}_{4/3};\Omega}, \quad \text{and} \quad \|\vec{\mathbf{v}}\|_{\mathcal{Q}} := \|\mathbf{v}\|_{0,4;\Omega} + \|\boldsymbol{\xi}\|_{0,\Omega}.$$

Hence, proceeding as in [12, eq. (3.15)], that is, by multiplying the first three equations of (2.8) by suitable test functions, using the integrating by parts formula (1.3), (2.4) and the Dirichlet boundary condition for  $\mathbf{u}$ , we arrive at the following mixed variational formulation of (2.8): Given  $p \in \mathbf{L}_{\kappa}^2(\Omega)$ , find  $(\mathbf{D}, \boldsymbol{\sigma}, \vec{\mathbf{u}}) \in \mathcal{H}_1 \times \mathcal{H}_2 \times \mathcal{Q}$  such that:

$$\begin{aligned}
[\mathcal{A}_p(\mathbf{D}), \mathbf{E}] + \mathcal{B}_1(\mathbf{E}, \boldsymbol{\sigma}) &= \mathcal{F}_{\mathbf{u}}(\mathbf{E}) \quad \forall \mathbf{E} \in \mathcal{H}_1, \\
\mathcal{B}_1(\mathbf{D}, \boldsymbol{\tau}) + \mathcal{B}(\boldsymbol{\tau}, \vec{\mathbf{u}}) &= \mathcal{G}(\boldsymbol{\tau}) \quad \forall \boldsymbol{\tau} \in \mathcal{H}_2, \\
\mathcal{B}(\boldsymbol{\sigma}, \vec{\mathbf{v}}) &= \mathcal{F}(\vec{\mathbf{v}}) \quad \forall \vec{\mathbf{v}} \in \mathcal{Q},
\end{aligned} \quad (2.11)$$

where the nonlinear operator  $\mathcal{A}_p : \mathcal{H}_1 \rightarrow \mathcal{H}'_1$ , the bilinear forms  $\mathcal{B}_1 : \mathcal{H}_1 \times \mathcal{H}_2 \rightarrow \mathbb{R}$  and  $\mathcal{B} : \mathcal{H}_2 \times \mathcal{Q} \rightarrow \mathbb{R}$ , and the functionals  $\mathcal{F}_{\mathbf{z}} : \mathcal{H}_1 \rightarrow \mathbb{R}$ , for each  $\mathbf{z} \in \mathbf{L}^4(\Omega)$ ,  $\mathcal{G} : \mathcal{H}_2 \rightarrow \mathbb{R}$ , and  $\mathcal{F} : \mathcal{Q} \rightarrow \mathbb{R}$ , are defined by

$$[\mathcal{A}_p(\mathbf{D}), \mathbf{E}] := \int_{\Omega} \eta(p, |\mathbf{D}|) \mathbf{D} : \mathbf{E} \quad \forall \mathbf{D}, \mathbf{E} \in \mathcal{H}_1, \quad (2.12)$$

$$\mathcal{B}_1(\mathbf{E}, \boldsymbol{\tau}) := - \int_{\Omega} \boldsymbol{\tau} : \mathbf{E} \quad \forall (\mathbf{E}, \boldsymbol{\tau}) \in \mathcal{H}_1 \times \mathcal{H}_2, \quad (2.13)$$

$$\mathcal{B}(\boldsymbol{\tau}, \vec{\mathbf{v}}) := - \int_{\Omega} \mathbf{v} \cdot \mathbf{div}(\boldsymbol{\tau}) - \int_{\Omega} \boldsymbol{\tau} : \boldsymbol{\xi} \quad \forall (\boldsymbol{\tau}, \vec{\mathbf{v}}) \in \mathcal{H}_2 \times \mathcal{Q}, \quad (2.14)$$

$$\mathcal{F}_{\mathbf{z}}(\mathbf{E}) := \rho \int_{\Omega} (\mathbf{z} \otimes \mathbf{z}) : \mathbf{E} \quad \forall \mathbf{E} \in \mathcal{H}_1, \quad (2.15)$$

$$\mathcal{G}(\boldsymbol{\tau}) := - \langle \boldsymbol{\tau} \boldsymbol{\nu}, \mathbf{u}_D \rangle \quad \forall \boldsymbol{\tau} \in \mathcal{H}_2, \quad (2.16)$$

and

$$\mathcal{F}(\vec{\mathbf{v}}) := \int_{\Omega} \mathbf{f} \cdot \mathbf{v} \quad \forall \vec{\mathbf{v}} \in \mathcal{Q}. \quad (2.17)$$

We recall from [12, Section 3] that, once the twofold saddle point-type problem (2.11) with the nonlinear operator  $\mathcal{A}_p$  is solved, the dependence on the given  $p$  requires updating the unknown pressure

according to the expression provided in the last row of (2.8). More precisely, noting that  $p \in L^2_\kappa(\Omega)$  and that the stress tensor in that equation is given by  $\boldsymbol{\sigma} + c_0 \mathbb{I}$  (cf. (2.9)), where  $\boldsymbol{\sigma} \in \mathbb{H}_0(\mathbf{div}_{4/3}; \Omega)$  is part of the solution of (2.11), and  $c_0$  is defined as

$$c_0 := \frac{1}{n|\Omega|} \int_\Omega \text{tr}(\boldsymbol{\sigma}) = -\frac{\kappa}{|\Omega|} - \frac{\rho}{n|\Omega|} \int_\Omega \text{tr}(\mathbf{u} \otimes \mathbf{u}),$$

we find that the pressure needs to be updated as follows (see [12, eq. (4.3)] for details)

$$p = -\frac{1}{n} \text{tr}(\boldsymbol{\sigma} + \rho(\mathbf{u} \otimes \mathbf{u})) + \frac{\kappa}{|\Omega|} + \frac{\rho}{n|\Omega|} \int_\Omega \text{tr}(\mathbf{u} \otimes \mathbf{u}). \quad (2.18)$$

The well-posedness of (2.11) is established in [12, Theorem 4.8], relying on a fixed-point strategy and a recent result for a class of twofold saddle-point operator equations in Banach spaces (cf. [16, Theorem 3.4]). More precisely, for a given  $\delta > 0$ , setting

$$\mathbf{W}(\delta) := \left\{ \mathbf{z} \in \mathbf{L}^4(\Omega) : \|\mathbf{z}\|_{0,4;\Omega} \leq \delta \right\} \quad \text{and} \quad \mathbf{S}(\delta) := \mathbf{W}(\delta) \times L^2_\kappa(\Omega),$$

and using suitable assumptions on  $\eta$  (cf. [12, eqs. (3.4), (4.7), and (4.8)]) along with smallness conditions on the data, specifically those detailed in [12, eqs. (4.17) and (4.33)], it is proved that an operator mapping  $\mathbf{S}(\delta)$  into itself has a unique fixed point  $(\mathbf{u}, p)$ . Equivalently, given this  $p \in L^2_\kappa(\Omega)$ , the system (2.11) has a unique solution  $(\mathbf{D}, \boldsymbol{\sigma}, \tilde{\mathbf{u}}) := (\mathbf{D}, \boldsymbol{\sigma}, (\mathbf{u}, \boldsymbol{\gamma})) \in \mathcal{H}_1 \times \mathcal{H}_2 \times \mathcal{Q}$ , with  $\mathbf{u} \in \mathbf{W}(\delta)$  and  $p$  satisfying (2.18).

### 2.3 The finite element methods

We let  $\{\mathcal{T}_h\}_{h>0}$  be a regular family of triangulations of  $\bar{\Omega}$ , which is made up of triangles  $K$  (when  $n = 2$ ) or tetrahedra (when  $n = 3$ ) of diameter  $h_K$ , and define the meshsize  $h := \max\{h_K : K \in \mathcal{T}_h\}$ . In turn, given an integer  $\ell \geq 0$  and  $K \in \mathcal{T}_h$ , we let  $\mathbf{P}_\ell(K)$  and  $\tilde{\mathbf{P}}_\ell(K)$  be the spaces of polynomials of degree  $\leq \ell$  and  $= \ell$ , respectively, defined on  $K$ , and denote its vector and tensor versions by  $\mathbf{P}_\ell(K) := [\mathbf{P}_\ell(K)]^n$  and  $\mathbb{P}_\ell(K) = [\mathbf{P}_\ell(K)]^{n \times n}$ , respectively. In addition, we let  $\mathbf{RT}_\ell(K) := \mathbf{P}_\ell(K) \oplus \tilde{\mathbf{P}}_\ell(K) \mathbf{x}$  be the local Raviart–Thomas space of order  $\ell$  defined on  $K$ , where  $\mathbf{x}$  stands for a generic vector in  $\mathbb{R}^n$ . Also, we let  $b_K$  be the bubble function on  $K$ , which is defined as the product of its  $n + 1$  barycentric coordinates. Then, we define the local bubble spaces of order  $\ell$  as

$$\mathbf{B}_\ell(K) := \mathbf{curl}(b_K \mathbf{P}_\ell(K)) \quad \text{if } n = 2, \quad \text{and} \quad \mathbf{B}_\ell(K) := \mathbf{curl}(b_K \mathbf{P}_\ell(K)) \quad \text{if } n = 3,$$

where  $\mathbf{curl}(v) := (\frac{\partial v}{\partial x_2}, -\frac{\partial v}{\partial x_1})$  if  $n = 2$  and  $v : K \rightarrow \mathbb{R}$ , and  $\mathbf{curl}(\mathbf{v}) := \nabla \times \mathbf{v}$  if  $n = 3$  and  $\mathbf{v} : K \rightarrow \mathbb{R}^3$ . The following global spaces are also needed

$$\mathbf{P}_\ell(\Omega) := \left\{ \mathbf{v}_h \in \mathbf{L}^2(\Omega) : \mathbf{v}_h|_K \in \mathbf{P}_\ell(K) \quad \forall K \in \mathcal{T}_h \right\},$$

$$\mathbb{P}_\ell(\Omega) := \left\{ \boldsymbol{\xi}_h \in \mathbb{L}^2(\Omega) : \boldsymbol{\xi}_h|_K \in \mathbb{P}_\ell(K) \quad \forall K \in \mathcal{T}_h \right\},$$

$$\mathbf{RT}_\ell(\Omega) := \left\{ \boldsymbol{\tau}_h \in \mathbb{H}(\mathbf{div}; \Omega) : \boldsymbol{\tau}_{h,i}|_K \in \mathbf{RT}_\ell(K) \quad \forall i \in \{1, \dots, n\}, \quad \forall K \in \mathcal{T}_h \right\},$$

and

$$\mathbb{B}_\ell(\Omega) := \left\{ \boldsymbol{\tau}_h \in \mathbb{H}(\mathbf{div}; \Omega) : \boldsymbol{\tau}_{h,i}|_K \in \mathbf{B}_\ell(K) \quad \forall i \in \{1, \dots, n\}, \quad \forall K \in \mathcal{T}_h \right\},$$

where  $\boldsymbol{\tau}_{h,i}$  stands for the  $i$ th-row of  $\boldsymbol{\tau}_h$ .

Now, we recall from [12, Section 6.3] two examples of stable finite element spaces  $\mathcal{H}_{1,h}$ ,  $\tilde{\mathcal{H}}_{2,h}$ ,  $\mathcal{Q}_{1,h}$ , and  $\mathcal{Q}_{2,h}$  satisfying the hypotheses required by the corresponding discrete analysis in [12, Section 5.2]. Indeed, the first example is based on the plane elasticity element with reduced symmetry (PEERS) of order  $\ell \geq 0$ , which, denoting  $\mathbb{C}(\bar{\Omega}) := [\mathbb{C}(\bar{\Omega})]^{n \times n}$ , is given by

$$\begin{aligned} \mathcal{H}_{1,h} &:= \mathbb{P}_{\ell+n}(\Omega) \cap \mathbb{L}_{\text{tr}}^2(\Omega), \quad \tilde{\mathcal{H}}_{2,h} := \mathbb{RT}_\ell(\Omega) \oplus \mathbb{B}_\ell(\Omega), \quad \mathcal{Q}_{1,h} := \mathbf{P}_\ell(\Omega), \\ \mathcal{Q}_{2,h} &:= \mathbb{C}(\bar{\Omega}) \cap \mathbb{P}_{\ell+1}(\Omega) \cap \mathbb{L}_{\text{sk}}^2(\Omega), \quad \text{and} \quad \mathcal{P}_h := \tilde{\mathcal{P}}_h \oplus \left\{ \frac{\kappa}{|\Omega|} \right\}, \end{aligned} \quad (2.19)$$

where  $\tilde{\mathcal{P}}_h := \mathbb{P}_{\bar{\ell}}(\Omega) \cap \mathbb{L}_0^2(\Omega)$  and  $\bar{\ell} := \max\{\ell+n, 2\ell\}$ . The second example is the Arnold–Falk–Winther (AFW)-based element of order  $\ell \geq 0$ , defined as

$$\begin{aligned} \mathcal{H}_{1,h} &:= \mathbb{P}_{\ell+1}(\Omega) \cap \mathbb{L}_{\text{tr}}^2(\Omega), \quad \tilde{\mathcal{H}}_{2,h} := \mathbb{P}_{\ell+1}(\Omega) \cap \mathbb{H}(\mathbf{div}; \Omega), \quad \mathcal{Q}_{1,h} := \mathbf{P}_\ell(\Omega), \\ \mathcal{Q}_{2,h} &:= \mathbb{P}_\ell(\Omega) \cap \mathbb{L}_{\text{sk}}^2(\Omega), \quad \text{and} \quad \mathcal{P}_h := \tilde{\mathcal{P}}_h \oplus \left\{ \frac{\kappa}{|\Omega|} \right\}, \end{aligned} \quad (2.20)$$

where  $\tilde{\mathcal{P}}_h := \mathbb{P}_{2\ell}(\Omega) \cap \mathbb{L}_0^2(\Omega)$ .

Thus, defining

$$\mathcal{H}_{2,h} := \mathbb{H}_0(\mathbf{div}_{4/3}; \Omega) \cap \tilde{\mathcal{H}}_{2,h} \quad \text{and} \quad \mathcal{Q}_h := \mathcal{Q}_{1,h} \times \mathcal{Q}_{2,h},$$

and letting  $p_h \in \mathcal{P}_h$  be a given discrete approximation of the pressure  $p$ , the Galerkin scheme for (2.11) reads: Find  $(\mathbf{D}_h, \boldsymbol{\sigma}_h, \bar{\mathbf{u}}_h) := (\mathbf{D}_h, \boldsymbol{\sigma}_h, (\mathbf{u}_h, \boldsymbol{\gamma}_h)) \in \mathcal{H}_{1,h} \times \mathcal{H}_{2,h} \times \mathcal{Q}_h$  such that

$$\begin{aligned} [\mathcal{A}_{p_h}(\mathbf{D}_h), \mathbf{E}_h] + \mathcal{B}_1(\mathbf{E}_h, \boldsymbol{\sigma}_h) &= \mathcal{F}_{\mathbf{u}_h}(\mathbf{E}_h) \quad \forall \mathbf{E}_h \in \mathcal{H}_{1,h}, \\ \mathcal{B}_1(\mathbf{D}_h, \boldsymbol{\tau}_h) + \mathcal{B}(\boldsymbol{\tau}_h, \bar{\mathbf{u}}_h) &= \mathcal{G}(\boldsymbol{\tau}_h) \quad \forall \boldsymbol{\tau}_h \in \mathcal{H}_{2,h}, \\ \mathcal{B}(\boldsymbol{\sigma}_h, \bar{\mathbf{v}}_h) &= \mathcal{F}(\bar{\mathbf{v}}_h) \quad \forall \bar{\mathbf{v}}_h \in \mathcal{Q}_h. \end{aligned} \quad (2.21)$$

We observe that, analogously to its continuous counterpart, the discrete pressure  $p_h$  is updated by following the discrete version of (2.18), that is:

$$p_h := -\frac{1}{n} \text{tr}(\boldsymbol{\sigma}_h + \rho(\mathbf{u}_h \otimes \mathbf{u}_h)) + \frac{\kappa}{|\Omega|} + \frac{\rho}{n|\Omega|} \int_{\Omega} \text{tr}(\mathbf{u}_h \otimes \mathbf{u}_h). \quad (2.22)$$

The solvability analysis and *a priori* error bounds for (2.21) are established in [12, Theorems 5.2, 5.3, and 6.2], respectively, considering both discrete approaches, (2.19) and (2.20). Indeed, similarly as remarked at the end of Section 2.2, and under the discrete analogues of the assumptions [12, eqs. (4.17) and (4.33)], which are detailed in [12, eqs. (5.15) and (5.17)], given  $\delta_d > 0$ , and setting

$$\mathbb{W}(\delta_d) := \left\{ \mathbf{z}_h \in \mathcal{Q}_{1,h} : \|\mathbf{z}_h\|_{0,4;\Omega} \leq \delta_d \right\} \quad \text{and} \quad \mathbb{S}(\delta_d) := \mathbb{W}(\delta_d) \times \mathcal{P}_h,$$

it is proved that a suitable discrete operator mapping  $\mathbb{S}(\delta_d)$  into itself, has a unique fixed point  $(\mathbf{u}_h, p_h)$  in it, which yields the unique solution  $(\mathbf{D}_h, \boldsymbol{\sigma}_h, \bar{\mathbf{u}}_h) := (\mathbf{D}_h, \boldsymbol{\sigma}_h, (\mathbf{u}_h, \boldsymbol{\gamma}_h)) \in \mathcal{H}_{1,h} \times \mathcal{H}_{2,h} \times \mathcal{Q}_h$  of (2.21), with  $\mathbf{u}_h \in \mathbb{W}(\delta_d)$  and  $p$  satisfying (2.22).

### 3 A residual-based a posteriori error estimator

In this section, we derive a reliable and efficient residual-based *a posteriori* error estimator for the two-dimensional version of the Galerkin scheme (2.21). The corresponding *a posteriori* error analysis

for the three-dimensional case, which follows from minor modifications of the analysis presented here, will be addressed in Appendix C. Throughout this section, we employ the notations and results from Appendix A.

Recalling that  $(\mathbf{D}_h, \boldsymbol{\sigma}_h, (\mathbf{u}_h, \boldsymbol{\gamma}_h)) \in \mathcal{H}_{1,h} \times \mathcal{H}_{2,h} \times \mathcal{Q}_h$  is the unique solution of the discrete problem (2.21), and that  $p_h$  is computed from (2.22), we define the global *a posteriori* error estimator  $\Theta$  as

$$\Theta = \left\{ \sum_{K \in \mathcal{T}_h} \Theta_{1,K}^{4/3} \right\}^{3/4} + \left\{ \sum_{K \in \mathcal{T}_h} \Theta_{2,K}^2 \right\}^{1/2} + \left\{ \sum_{K \in \mathcal{T}_h} \Theta_{3,K}^4 \right\}^{1/4}, \quad (3.1)$$

where, for each  $K \in \mathcal{T}_h$ , the local error indicators  $\Theta_{1,K}^{4/3}$ ,  $\Theta_{2,K}^2$  and  $\Theta_{3,K}^4$  are defined as

$$\Theta_{1,K}^{4/3} := \|\mathbf{f} + \mathbf{div}(\boldsymbol{\sigma}_h)\|_{0,4/3;K}^{4/3}, \quad (3.2)$$

$$\begin{aligned} \Theta_{2,K}^2 &:= \|\eta(p_h, |\mathbf{D}_h|) \mathbf{D}_h - \boldsymbol{\sigma}_h^d - \rho(\mathbf{u}_h \otimes \mathbf{u}_h)^d\|_{0,K}^2 + \|\boldsymbol{\sigma}_h - \boldsymbol{\sigma}_h^t\|_{0,K}^2 \\ &+ h_K^2 \|\mathbf{rot}(\mathbf{D}_h + \boldsymbol{\gamma}_h)\|_{0,K}^2 + \sum_{e \in \mathcal{E}_h(K) \cap \mathcal{E}(\Omega)} h_e \|\llbracket (\mathbf{D}_h + \boldsymbol{\gamma}_h) \mathbf{s} \rrbracket\|_{0,e}^2 \\ &+ \sum_{e \in \mathcal{E}_h(K) \cap \mathcal{E}(\Gamma)} h_e \|\nabla \mathbf{u}_D \mathbf{s} - (\mathbf{D}_h + \boldsymbol{\gamma}_h) \mathbf{s}\|_{0,e}^2, \end{aligned} \quad (3.3)$$

and

$$\Theta_{3,K}^4 := h_K^4 \|\nabla \mathbf{u}_h - (\mathbf{D}_h + \boldsymbol{\gamma}_h)\|_{0,4;K}^4 + \sum_{e \in \mathcal{E}_h(K) \cap \mathcal{E}(\Gamma)} h_e \|\mathbf{u}_D - \mathbf{u}_h\|_{0,4;e}^4. \quad (3.4)$$

Notice that the last term defining  $\Theta_{2,K}^2$  (cf. (3.3)) requires that  $(\nabla \mathbf{u}_D \mathbf{s})|_e \in \mathbf{L}^2(e)$  for all  $e \in \mathcal{E}(\Gamma)$ , which is guaranteed by simply assuming that  $\mathbf{u}_D \in \mathbf{H}^1(\Gamma)$ . Nevertheless, to be more precise, it suffices to assume that  $\nabla \mathbf{u}_D|_\Gamma \in \mathbb{L}^2(\Gamma)$ , which holds if  $\nabla \mathbf{u}_D|_\Gamma$  coincides with the trace of the gradient of a function in  $\mathbf{H}^t(\Omega)$  for some  $t > 4/3$ . In any case, the Dirichlet data used in the numerical results reported below in Section 4 satisfy the first-mentioned assumptions on  $\mathbf{u}_D$ .

From now on, we define

$$\|\vec{\mathbf{D}} - \vec{\mathbf{D}}_h\|_{\mathcal{H}} := \|\mathbf{D} - \mathbf{D}_h\|_{\mathcal{H}_1} + \|\boldsymbol{\sigma} - \boldsymbol{\sigma}_h\|_{\mathcal{H}_2} + \|\vec{\mathbf{u}} - \vec{\mathbf{u}}_h\|_{\mathcal{Q}},$$

where  $\vec{\mathbf{D}} := (\mathbf{D}, \boldsymbol{\sigma}, \vec{\mathbf{u}}) \in \mathcal{H} := \mathcal{H}_1 \times \mathcal{H}_2 \times \mathcal{Q}$  and  $\vec{\mathbf{D}}_h := (\mathbf{D}_h, \boldsymbol{\sigma}_h, \vec{\mathbf{u}}_h) \in \mathcal{H}_h := \mathcal{H}_{1,h} \times \mathcal{H}_{2,h} \times \mathcal{Q}_h$  denote the unique solutions of (2.11) and (2.21), respectively. The main goal of this section is to establish, under suitable assumptions, the existence of positive constants  $C_{\text{eff}}$  and  $C_{\text{rel}}$ , independent of the mesh sizes and the continuous and discrete solutions, such that

$$C_{\text{eff}} \Theta + \text{h.o.t} \leq \|\vec{\mathbf{D}} - \vec{\mathbf{D}}_h\|_{\mathcal{H}} + \|p - p_h\|_{0,\Omega} \leq C_{\text{rel}} \Theta, \quad (3.5)$$

where *h.o.t* is a generic expression denoting one or several terms of higher order, whereas  $p$  and  $p_h$  are computed according to (2.18) and (2.22), respectively. The upper and lower bounds in (3.5), which are known as the reliability and efficiency of  $\Theta$ , are derived below in Sections 3.1 and 3.2, respectively.

### 3.1 Reliability

The main result of this section is stated in the following theorem. To this end, and as done in [12, eq. (5.19)], given  $r \in \mathbb{L}^2_\kappa(\Omega)$ , we first note that we can define the operator  $\Xi_r : \mathcal{H} \rightarrow \mathcal{H}'$ , which arises from the left-hand side of the variational formulation (2.11) after summing all its rows, that is,

$$[\Xi_r(\vec{\mathbf{C}}), \vec{\mathbf{E}}] := [\mathcal{A}_r(\mathbf{C}), \mathbf{E}] + \mathcal{B}_1(\mathbf{E}, \boldsymbol{\zeta}) + \mathcal{B}_1(\mathbf{C}, \boldsymbol{\tau}) + \mathcal{B}(\boldsymbol{\tau}, \vec{\mathbf{w}}) + \mathcal{B}(\boldsymbol{\zeta}, \vec{\mathbf{v}}), \quad (3.6)$$

for all  $\vec{\mathbf{C}} := (\mathbf{C}, \zeta, \vec{\mathbf{w}})$ ,  $\vec{\mathbf{E}} := (\mathbf{E}, \boldsymbol{\tau}, \vec{\mathbf{v}}) \in \mathcal{H}$ , so that (2.11) can be rewritten as

$$[\Xi_p(\vec{\mathbf{D}}), \vec{\mathbf{E}}] = \mathcal{F}_{\mathbf{u}}(\mathbf{E}) + \mathcal{G}(\boldsymbol{\tau}) + \mathcal{F}(\vec{\mathbf{v}}) \quad \forall \vec{\mathbf{E}} \in \mathcal{H}. \quad (3.7)$$

Thus, the smoothness of the regularized function  $\eta$  (cf. (2.3)) allows to show that for each  $r \in \mathbb{L}_{\kappa}^2(\Omega)$ , the operator  $\mathcal{A}_r$  (cf. (2.12)), and hence  $\Xi_r$  as well, have first order Gâteaux derivatives  $\mathcal{D}(\mathcal{A}_r) \in \mathcal{L}(\mathcal{H}_1, \mathcal{L}(\mathcal{H}_1, \mathcal{H}'_1))$  and  $\mathcal{D}(\Xi_r) \in \mathcal{L}(\mathcal{H}, \mathcal{L}(\mathcal{H}, \mathcal{H}'))$ , respectively. Moreover, using [12, eqs. (4.9) and (4.10) in Lemma 4.2], one is able to prove (see, e.g. [27, Lemma 3.1]) that for each  $\mathbf{C} \in \mathcal{H}_1$ , the operator  $\mathcal{D}(\mathcal{A}_r)(\mathbf{C}) \in \mathcal{L}(\mathcal{H}_1, \mathcal{H}'_1)$  can be identified as a bounded and  $\mathcal{H}_1$ -elliptic bilinear form with constants  $L_{\mathcal{A}}$  and  $\alpha_{\mathcal{A}}$ , respectively. It follows that for each  $r \in \mathbb{L}_{\kappa}^2(\Omega)$ , and for each  $\vec{\mathbf{C}} \in \mathcal{H}$ , the operator  $\mathcal{D}(\Xi_r)(\vec{\mathbf{C}}) \in \mathcal{L}(\mathcal{H}, \mathcal{H}')$  satisfies the hypotheses of the linear version of [12, Theorem 4.1], and hence, there exists a positive constant  $\alpha_{\Xi}$ , depending only on  $L_{\mathcal{A}}$ ,  $\alpha_{\mathcal{A}}$ , and the inf-sup constants of  $\mathcal{B}$  and  $\mathcal{B}_1$ , namely  $\tilde{\beta}$  and  $\tilde{\beta}_1$  (cf. [12, eqs. (4.12), (4.13)]), such that the following global inf-sup condition holds:

$$\alpha_{\Xi} \|\vec{\mathbf{F}}\|_{\mathcal{H}} \leq \sup_{\mathbf{0} \neq \vec{\mathbf{E}} \in \mathcal{H}} \frac{\mathcal{D}(\Xi_r)(\vec{\mathbf{C}})(\vec{\mathbf{F}}, \vec{\mathbf{E}})}{\|\vec{\mathbf{E}}\|_{\mathcal{H}}} \quad \forall \vec{\mathbf{F}} \in \mathcal{H}. \quad (3.8)$$

In addition, we let

$$C_{1,\Xi} := \alpha_{\Xi}^{-1} n^{-1/2} \quad \text{and} \quad C_{2,\Xi} := \alpha_{\Xi}^{-1} \rho (2 n^{-1/2} L_{\eta} + 1), \quad (3.9)$$

where  $\alpha_{\Xi}$  satisfies (3.8), and  $L_{\eta}$  denotes the Lipschitz continuity constant of  $\eta$  (cf. [12, eq. (4.8)]).

The aforementioned result is stated now.

**Theorem 3.1.** *Assume that  $L_{\eta}$  and the radii  $\delta$  and  $\delta_{\mathbf{d}}$  are sufficiently small so that*

$$C_{1,\Xi} L_{\eta} \leq \frac{1}{2} \quad \text{and} \quad C_{2,\Xi} n^{1/2} (\delta + \delta_{\mathbf{d}}) \leq \frac{1}{2}. \quad (3.10)$$

*Then, there exists a constant  $C_{\text{rel}} > 0$ , such that*

$$\|\vec{\mathbf{D}} - \vec{\mathbf{D}}_h\|_{\mathcal{H}} + \|p - p_h\|_{0,\Omega} \leq C_{\text{rel}} \Theta. \quad (3.11)$$

We begin the proof of Theorem 3.1 with a preliminary lemma. Specifically, proceeding analogously to [13, Section 3.1] (see also [20, Section 1]), we first introduce the residual functional  $\mathcal{R} : \mathcal{H} \rightarrow \mathbb{R}$ , given by

$$\mathcal{R}(\vec{\mathbf{E}}) := \mathcal{R}_1(\mathbf{E}) + \mathcal{R}_2(\boldsymbol{\tau}) + \mathcal{R}_3(\vec{\mathbf{v}}) \quad \forall \vec{\mathbf{E}} = (\mathbf{E}, \boldsymbol{\tau}, \vec{\mathbf{v}}) \in \mathcal{H}, \quad (3.12)$$

where  $\mathcal{R}_1 : \mathcal{H}_1 \rightarrow \mathbb{R}$ ,  $\mathcal{R}_2 : \mathcal{H}_2 \rightarrow \mathbb{R}$ , and  $\mathcal{R}_3 : \mathcal{Q} \rightarrow \mathbb{R}$  are given by

$$\mathcal{R}_1(\mathbf{E}) := \mathcal{F}_{\mathbf{u}_h}(\mathbf{E}) - [\mathcal{A}_{p_h}(\mathbf{D}_h), \mathbf{E}] - \mathcal{B}_1(\mathbf{E}, \boldsymbol{\sigma}_h) \quad \forall \mathbf{E} \in \mathcal{H}_1, \quad (3.13)$$

$$\mathcal{R}_2(\boldsymbol{\tau}) := \mathcal{G}(\boldsymbol{\tau}) - \mathcal{B}_1(\mathbf{D}_h, \boldsymbol{\tau}) - \mathcal{B}(\boldsymbol{\tau}, \vec{\mathbf{u}}_h) \quad \forall \boldsymbol{\tau} \in \mathcal{H}_2, \quad (3.14)$$

and

$$\mathcal{R}_3(\vec{\mathbf{v}}) := \mathcal{F}(\vec{\mathbf{v}}) - \mathcal{B}(\boldsymbol{\sigma}_h, \vec{\mathbf{v}}) \quad \forall \vec{\mathbf{v}} \in \mathcal{Q}, \quad (3.15)$$

respectively, which according to the discrete problem (2.21) satisfy

$$\mathcal{R}_1(\mathbf{E}_h) = 0 \quad \forall \mathbf{E}_h \in \mathcal{H}_{1,h}, \quad \mathcal{R}_2(\boldsymbol{\tau}_h) = 0 \quad \forall \boldsymbol{\tau}_h \in \mathcal{H}_{2,h}, \quad \text{and} \quad \mathcal{R}_3(\vec{\mathbf{v}}_h) = 0 \quad \forall \vec{\mathbf{v}}_h \in \mathcal{Q}_h. \quad (3.16)$$

We are now in a position to establish the following aforementioned preliminary *a posteriori* error estimate.

**Lemma 3.2.** *Assume that  $L_\eta$  and the radii  $\delta$  and  $\delta_d$  satisfy (3.10). Then, there exists a positive constant  $C$ , independent of  $h$ , such that*

$$\|\vec{\mathbf{D}} - \vec{\mathbf{D}}_h\|_{\mathcal{H}} + \|p - p_h\|_{0,\Omega} \leq C \left\{ \|\mathcal{R}_1\|_{\mathcal{H}'_1} + \|\mathcal{R}_2\|_{\mathcal{H}'_2} + \|\mathcal{R}_3\|_{\mathcal{Q}'} \right\}. \quad (3.17)$$

*Proof.* We begin by proceeding analogously to the proof of [27, Theorem 3.3]. In fact, given  $p \in L^2_\kappa(\Omega)$  satisfying (2.18) and since  $\vec{\mathbf{D}}$  and  $\vec{\mathbf{D}}_h$  belong to  $\mathcal{H}$ , a straightforward application of the mean value theorem yields the existence of a convex combination of  $\vec{\mathbf{D}}$  and  $\vec{\mathbf{D}}_h$ , say  $\vec{\mathbf{C}}_h \in \mathcal{H}$ , such that

$$\mathcal{D}(\Xi_p)(\vec{\mathbf{C}}_h)(\vec{\mathbf{D}} - \vec{\mathbf{D}}_h, \vec{\mathbf{E}}) = [\Xi_p(\vec{\mathbf{D}}), \vec{\mathbf{E}}] - [\Xi_p(\vec{\mathbf{D}}_h), \vec{\mathbf{E}}] \quad \forall \vec{\mathbf{E}} \in \mathcal{H}. \quad (3.18)$$

Then, by adding and subtracting  $[\Xi_{p_h}(\vec{\mathbf{D}}_h), \vec{\mathbf{E}}]$  and  $\mathcal{F}_{\mathbf{u}_h}(\mathbf{E})$  on the right-hand side of (3.18), using (3.7), and the definitions of  $\Xi_p$  and  $\mathcal{R}$  (cf. (3.6), (3.12)), along with straightforward algebraic manipulations, we deduce that

$$\mathcal{D}(\Xi_p)(\vec{\mathbf{C}}_h)(\vec{\mathbf{D}} - \vec{\mathbf{D}}_h, \vec{\mathbf{E}}) = \mathcal{R}(\vec{\mathbf{E}}) + (\mathcal{F}_{\mathbf{u}} - \mathcal{F}_{\mathbf{u}_h})(\mathbf{E}) - [\mathcal{A}_p(\mathbf{D}_h) - \mathcal{A}_{p_h}(\mathbf{D}_h), \mathbf{E}] \quad \forall \vec{\mathbf{E}} \in \mathcal{H}. \quad (3.19)$$

In turn, applying (3.8) with  $r = p$ ,  $\vec{\mathbf{C}} = \vec{\mathbf{C}}_h$ , and  $\vec{\mathbf{F}} = \vec{\mathbf{D}} - \vec{\mathbf{D}}_h$ , using (3.19) and the continuity of the operator  $\mathcal{A}_p$  (cf. [12, eq. (4.11) in Lemma 4.2]), with the positive continuity constant  $L_\eta$ , we get

$$\alpha_\Xi \|\vec{\mathbf{D}} - \vec{\mathbf{D}}_h\|_{\mathcal{H}} \leq \|\mathcal{R}\|_{\mathcal{H}'} + \|\mathcal{F}_{\mathbf{u}} - \mathcal{F}_{\mathbf{u}_h}\|_{\mathcal{H}'_1} + L_\eta \|p - p_h\|_{0,\Omega}. \quad (3.20)$$

Next, we focus on bounding the last two terms on the right-hand side of (3.20). First, using the definition of  $\mathcal{F}_{\mathbf{z}}$  (cf. (2.15)) and applying the Cauchy–Schwarz inequality, we obtain

$$\|\mathcal{F}_{\mathbf{u}} - \mathcal{F}_{\mathbf{u}_h}\|_{\mathcal{H}'_1} \leq \rho \|\mathbf{u} \otimes \mathbf{u} - \mathbf{u}_h \otimes \mathbf{u}_h\|_{0,\Omega}, \quad (3.21)$$

whereas, according to the expressions provided by (2.18) and (2.22), and proceeding similarly to [12, eq. (5.31)], the last term in (3.20) can be bounded by

$$\|p - p_h\|_{0,\Omega} \leq n^{-1/2} \left\{ \|\boldsymbol{\sigma} - \boldsymbol{\sigma}_h\|_{0,\Omega} + 2\rho \|\mathbf{u} \otimes \mathbf{u} - \mathbf{u}_h \otimes \mathbf{u}_h\|_{0,\Omega} \right\}. \quad (3.22)$$

Furthermore, subtracting and adding the term  $(\mathbf{u} \otimes \mathbf{u}_h)$ , using Cauchy–Schwarz’s inequality and the fact that  $\mathbf{u} \in \mathbf{W}(\delta)$  and  $\mathbf{u}_h \in \mathbf{W}(\delta_d)$ , there holds

$$\|\mathbf{u} \otimes \mathbf{u} - \mathbf{u}_h \otimes \mathbf{u}_h\|_{0,\Omega} \leq n^{1/2} (\|\mathbf{u}\|_{0,4;\Omega} + \|\mathbf{u}_h\|_{0,4;\Omega}) \|\mathbf{u} - \mathbf{u}_h\|_{0,4;\Omega} \leq n^{1/2} (\delta + \delta_d) \|\mathbf{u} - \mathbf{u}_h\|_{0,4;\Omega}, \quad (3.23)$$

whence, combining (3.20) with (3.21), (3.22), and (3.23), and using the definition of the constants  $C_{1,\Xi}, C_{2,\Xi}$  (cf. (3.9)), we obtain

$$\|\vec{\mathbf{D}} - \vec{\mathbf{D}}_h\|_{\mathcal{H}} \leq \frac{1}{\alpha_\Xi} \|\mathcal{R}\|_{\mathcal{H}'} + C_{1,\Xi} L_\eta \|\boldsymbol{\sigma} - \boldsymbol{\sigma}_h\|_{0,\Omega} + C_{2,\Xi} n^{1/2} (\delta + \delta_d) \|\mathbf{u} - \mathbf{u}_h\|_{0,4;\Omega}. \quad (3.24)$$

Thus, by employing (3.10) in (3.24) and the definition of the residual  $\mathcal{R}$  (cf. (3.12)) in terms of  $\mathcal{R}_1$ ,  $\mathcal{R}_2$ , and  $\mathcal{R}_3$  (cf. (3.13), (3.14), (3.15)), we find that

$$\|\vec{\mathbf{D}} - \vec{\mathbf{D}}_h\|_{\mathcal{H}} \leq \frac{2}{\alpha_\Xi} \left\{ \|\mathcal{R}_1\|_{\mathcal{H}'_1} + \|\mathcal{R}_2\|_{\mathcal{H}'_2} + \|\mathcal{R}_3\|_{\mathcal{Q}'} \right\}, \quad (3.25)$$

so that the corresponding estimate for  $\|p - p_h\|_{0,\Omega}$  follows from (3.22), (3.23), and (3.25), thus yielding (3.17), which concludes the proof.  $\square$

Throughout the rest of this section, we provide suitable upper bounds for each one of the terms on the right-hand side of (3.17). We begin by establishing the corresponding estimates for  $\|\mathcal{R}_1\|_{\mathcal{H}'_1}$  and  $\|\mathcal{R}_3\|_{\mathcal{Q}'}$  (cf. (3.13) and (3.15)).

**Lemma 3.3.** *There hold*

$$\|\mathcal{R}_1\|_{\mathcal{H}'_1} \leq \|\eta(p_h, |\mathbf{D}_h|) \mathbf{D}_h - \boldsymbol{\sigma}_h^d - \rho(\mathbf{u}_h \otimes \mathbf{u}_h)^d\|_{0;\Omega} \quad (3.26)$$

and

$$\|\mathcal{R}_3\|_{\mathcal{Q}'} \leq \|\mathbf{f} + \mathbf{div}(\boldsymbol{\sigma}_h)\|_{0,4/3;\Omega} + \frac{1}{2} \|\boldsymbol{\sigma}_h - \boldsymbol{\sigma}_h^t\|_{0,\Omega}. \quad (3.27)$$

*Proof.* First, using the definition of the functionals and operators  $\mathcal{R}_1$ ,  $\mathcal{F}_{\mathbf{u}_h}$ ,  $\mathcal{A}_{p_h}$ , and  $\mathcal{B}_1$  (cf. (3.13), (2.15), (2.12), (2.13)), along with the fact that  $\boldsymbol{\tau}^d : \mathbf{E} = \boldsymbol{\tau} : \mathbf{E}$ , for all  $\mathbf{E} \in \mathcal{H}_1$  (cf. (2.10)), and Cauchy–Schwarz’s inequality, we deduce that

$$\begin{aligned} |\mathcal{R}_1(\mathbf{E})| &= \left| - \int_{\Omega} \left( \eta(p_h, |\mathbf{D}_h|) \mathbf{D}_h - \boldsymbol{\sigma}_h^d - \rho(\mathbf{u}_h \otimes \mathbf{u}_h)^d \right) : \mathbf{E} \right| \\ &\leq \|\eta(p_h, |\mathbf{D}_h|) \mathbf{D}_h - \boldsymbol{\sigma}_h^d - \rho(\mathbf{u}_h \otimes \mathbf{u}_h)^d\|_{0,\Omega} \|\mathbf{E}\|_{0,\Omega}, \end{aligned}$$

which yields (3.26). On the other hand, employing the definition of the functionals and bilinear form  $\mathcal{R}_3$ ,  $\mathcal{F}$ , and  $\mathcal{B}$  (cf. (3.15), (2.17), (2.14)), in conjunction with the decomposition of the tensor  $\boldsymbol{\sigma}_h$  into

$$\boldsymbol{\sigma}_h = \frac{1}{2} (\boldsymbol{\sigma}_h + \boldsymbol{\sigma}_h^t) + \frac{1}{2} (\boldsymbol{\sigma}_h - \boldsymbol{\sigma}_h^t),$$

the fact that  $(\boldsymbol{\sigma}_h + \boldsymbol{\sigma}_h^t) : \boldsymbol{\xi} = \mathbf{0}$ , for all  $\boldsymbol{\xi} \in \mathbb{L}_{\text{sk}}^2(\Omega)$ , and the Cauchy–Schwarz and Hölder inequalities, we obtain

$$\begin{aligned} |\mathcal{R}_3(\vec{\mathbf{v}})| &= \left| \int_{\Omega} (\mathbf{f} + \mathbf{div}(\boldsymbol{\sigma}_h)) \cdot \mathbf{v} + \frac{1}{2} \int_{\Omega} (\boldsymbol{\sigma}_h - \boldsymbol{\sigma}_h^t) : \boldsymbol{\xi} \right| \\ &\leq \|\mathbf{f} + \mathbf{div}(\boldsymbol{\sigma}_h)\|_{0,4/3;\Omega} \|\mathbf{v}\|_{0,4;\Omega} + \frac{1}{2} \|\boldsymbol{\sigma}_h - \boldsymbol{\sigma}_h^t\|_{0,\Omega} \|\boldsymbol{\xi}\|_{0,\Omega}, \end{aligned}$$

which implies (3.27) and ends the proof.  $\square$

We now turn to the derivation of the corresponding estimate for  $\|\mathcal{R}_2\|_{\mathcal{H}'_2}$ . To that end, we first recall from (3.16) that  $\mathcal{R}_2(\boldsymbol{\tau}_h) = 0$  for all  $\boldsymbol{\tau}_h \in \mathcal{H}_{2,h}$ , whence in the computation of

$$\|\mathcal{R}_2\|_{\mathcal{H}'_2} := \sup_{\mathbf{0} \neq \boldsymbol{\tau} \in \mathcal{H}_2} \frac{\mathcal{R}_2(\boldsymbol{\tau})}{\|\boldsymbol{\tau}\|_{\mathcal{H}_2}}, \quad (3.28)$$

we can replace each term  $\mathcal{R}_2(\boldsymbol{\tau})$  by  $\mathcal{R}_2(\boldsymbol{\tau} - \boldsymbol{\tau}_h)$ , with a suitable  $\boldsymbol{\tau}_h \in \mathcal{H}_{2,h}$  (cf. (2.19), (2.20)) depending on the given  $\boldsymbol{\tau} \in \mathcal{H}_2$ . Indeed, we first consider the Helmholtz decomposition (A.10) provided by Lemma A.2, with  $p = 4/3$ , which says that for each  $\boldsymbol{\tau} \in \mathcal{H}_2$  there exist  $\boldsymbol{\zeta} \in \mathbb{W}^{1,4/3}(\Omega)$  and  $\boldsymbol{\xi} \in \mathbf{H}^1(\Omega)$ , such that

$$\boldsymbol{\tau} = \boldsymbol{\zeta} + \mathbf{curl}(\boldsymbol{\xi}) \quad \text{in } \Omega \quad \text{and} \quad \|\boldsymbol{\zeta}\|_{1,4/3;\Omega} + \|\boldsymbol{\xi}\|_{1,\Omega} \leq C_{4/3} \|\boldsymbol{\tau}\|_{\mathbf{div}_{4/3;\Omega}}, \quad (3.29)$$

with a positive constant  $C_{4/3}$  independent of  $\boldsymbol{\tau}$ . Next, for simplicity of presentation, we focus on the discrete approach (2.19), which relies on PEERS-based elements of order  $\ell \geq 0$ . The AFW-based discretization (2.20) can be handled analogously, using the BDM interpolation operator instead of the Raviart–Thomas one. In fact, setting

$$\boldsymbol{\tau}_h := \boldsymbol{\Pi}_h^k(\boldsymbol{\zeta}) + \mathbf{curl}(\mathcal{I}_h(\boldsymbol{\xi})) + c\mathbb{I}, \quad (3.30)$$

where  $\mathbf{\Pi}_h^k$  and  $\mathcal{I}_h$  denote the tensor and vector versions of the Raviart–Thomas (or BDM, in the case of the AFW-based approach) and Clément interpolation operators, respectively (cf. Appendix A). The constant  $c$  is chosen so that  $\text{tr}(\boldsymbol{\tau}_h)$  has zero mean value, and hence  $\boldsymbol{\tau}_h$  belongs to  $\mathcal{H}_{2,h}$ . Note that  $\mathbf{\Pi}_h^k(\boldsymbol{\zeta})$  lies in  $\mathbb{RT}_\ell(\Omega) \subseteq \tilde{\mathcal{H}}_{2,h}$  (cf. (2.19)). Also observe that  $\boldsymbol{\tau}_h$  can be interpreted as a discrete Helmholtz decomposition of  $\boldsymbol{\tau}$ . In this way, using the second equation of the Galerkin scheme (2.21), together with the compatibility condition (2.4), we deduce that  $\mathcal{R}_2(c\mathbb{I}) = 0$ , so that denoting

$$\hat{\boldsymbol{\zeta}} := \boldsymbol{\zeta} - \mathbf{\Pi}_h^k(\boldsymbol{\zeta}) \quad \text{and} \quad \hat{\boldsymbol{\xi}} := \boldsymbol{\xi} - \mathcal{I}_h(\boldsymbol{\xi}),$$

it follows from (3.29) and (3.30), that

$$\mathcal{R}_2(\boldsymbol{\tau}) = \mathcal{R}_2(\boldsymbol{\tau} - \boldsymbol{\tau}_h) = \mathcal{R}_2(\hat{\boldsymbol{\zeta}}) + \mathcal{R}_2(\mathbf{curl}(\hat{\boldsymbol{\xi}})), \quad (3.31)$$

where, bearing in mind the definition of  $\mathcal{R}_2$  (cf. (3.14), (2.16)), we find that

$$\mathcal{R}_2(\hat{\boldsymbol{\zeta}}) := \int_{\Omega} (\mathbf{D}_h + \boldsymbol{\gamma}_h) : \hat{\boldsymbol{\zeta}} + \int_{\Omega} \mathbf{u}_h \cdot \mathbf{div}(\hat{\boldsymbol{\zeta}}) - \langle \hat{\boldsymbol{\zeta}} \boldsymbol{\nu}, \mathbf{u}_D \rangle \quad (3.32)$$

and

$$\mathcal{R}_2(\mathbf{curl}(\hat{\boldsymbol{\xi}})) := \int_{\Omega} (\mathbf{D}_h + \boldsymbol{\gamma}_h) : \mathbf{curl}(\hat{\boldsymbol{\xi}}) - \langle \mathbf{curl}(\hat{\boldsymbol{\xi}}) \boldsymbol{\nu}, \mathbf{u}_D \rangle. \quad (3.33)$$

The following lemma establishes the residual upper bound for  $\|\mathcal{R}_2\|_{\mathcal{H}'_2}$ .

**Lemma 3.4.** *Assume that  $\mathbf{u}_D \in \mathbf{H}^1(\Gamma)$ . Then, there exists a positive constant  $C$ , independent of  $h$ , such that*

$$\|\mathcal{R}_2\|_{\mathcal{H}'_2} \leq C \left\{ \left( \sum_{K \in \mathcal{T}_h} \tilde{\Theta}_K^2 \right)^{1/2} + \left( \sum_{K \in \mathcal{T}_h} \Theta_{3,K}^4 \right)^{1/4} \right\}. \quad (3.34)$$

where  $\Theta_{3,K}$  is defined in (3.4), and

$$\begin{aligned} \tilde{\Theta}_K^2 &:= h_K^2 \|\mathbf{rot}(\mathbf{D}_h + \boldsymbol{\gamma}_h)\|_{0,K}^2 + \sum_{e \in \mathcal{E}_h(K)} h_e \|\llbracket (\mathbf{D}_h + \boldsymbol{\gamma}_h) \mathbf{s} \rrbracket\|_{0,e}^2 \\ &+ \sum_{e \in \mathcal{E}_h(K) \cap \mathcal{E}_h(\Gamma)} h_e \|\nabla \mathbf{u}_D \mathbf{s} - (\mathbf{D}_h + \boldsymbol{\gamma}_h) \mathbf{s}\|_{0,e}^2. \end{aligned}$$

*Proof.* We proceed as in [13, Lemma 3.6]. In fact, according to (3.31), we begin by estimating  $\mathcal{R}_2(\hat{\boldsymbol{\zeta}})$ . Let us first observe that, for each  $e \in \mathcal{E}_h$ , the identity (A.3) and the fact that  $\mathbf{u}_h|_e \in \mathbf{P}_k(e)$ , yield  $\int_e \hat{\boldsymbol{\zeta}} \boldsymbol{\nu} \cdot \mathbf{u}_h = 0$ . Hence, locally integrating by parts the second term in (3.32), we readily obtain

$$\mathcal{R}_2(\hat{\boldsymbol{\zeta}}) = - \sum_{K \in \mathcal{T}_h} \int_K \left\{ \nabla \mathbf{u}_h - (\mathbf{D}_h + \boldsymbol{\gamma}_h) \right\} : \hat{\boldsymbol{\zeta}} - \sum_{e \in \mathcal{E}_h(\Gamma)} \int_e (\mathbf{u}_D - \mathbf{u}_h) \cdot \hat{\boldsymbol{\zeta}} \boldsymbol{\nu}.$$

Thus, applying the Hölder inequality along with the approximation properties of  $\mathbf{\Pi}_h^k$  (cf. (A.8)–(A.9) in Lemma A.1) with  $p = 4/3$  and  $l = 0$ , and the stability estimate from (3.29), we get

$$|\mathcal{R}_2(\hat{\boldsymbol{\zeta}})| \leq \hat{C}_1 \left\{ \sum_{K \in \mathcal{T}_h} h_K^4 \|\nabla \mathbf{u}_h - (\mathbf{D}_h + \boldsymbol{\gamma}_h)\|_{0,4;K}^4 + \sum_{e \in \mathcal{E}_h(\Gamma)} h_e \|\mathbf{u}_D - \mathbf{u}_h\|_{0,4;e}^4 \right\}^{1/4} \|\boldsymbol{\tau}\|_{\text{div}_{4/3};\Omega}. \quad (3.35)$$

Next, we estimate  $\mathcal{R}_2(\underline{\mathbf{curl}}(\widehat{\boldsymbol{\xi}}))$  (cf. (3.33)). In fact, regarding its second term, a suitable boundary integration by parts formula (cf. [21, eq. (3.35) in Lemma 3.5]) yields

$$\langle \underline{\mathbf{curl}}(\widehat{\boldsymbol{\xi}})\boldsymbol{\nu}, \mathbf{u}_D \rangle_\Gamma = -\langle \nabla \mathbf{u}_D \mathbf{s}, \widehat{\boldsymbol{\xi}} \rangle_\Gamma. \quad (3.36)$$

In turn, locally integrating by parts the first term of  $\mathcal{R}_2(\underline{\mathbf{curl}}(\widehat{\boldsymbol{\xi}}))$ , we get

$$\begin{aligned} & \int_\Omega (\mathbf{D}_h + \boldsymbol{\gamma}_h) : \underline{\mathbf{curl}}(\widehat{\boldsymbol{\xi}}) \\ &= \sum_{K \in \mathcal{T}_h} \int_K \mathbf{rot}(\mathbf{D}_h + \boldsymbol{\gamma}_h) \cdot \widehat{\boldsymbol{\xi}} - \sum_{e \in \mathcal{E}_h(\Omega)} \int_e \llbracket (\mathbf{D}_h + \boldsymbol{\gamma}_h) \mathbf{s} \rrbracket \cdot \widehat{\boldsymbol{\xi}} - \sum_{e \in \mathcal{E}_h(\Gamma)} \int_e (\mathbf{D}_h + \boldsymbol{\gamma}_h) \mathbf{s} \cdot \widehat{\boldsymbol{\xi}}, \end{aligned}$$

which together with (3.36), the Cauchy–Schwarz inequality, the approximation properties of  $\mathcal{I}_h$  (cf. Lemma A.3), and again the stability estimate from (3.29), implies

$$\begin{aligned} |\mathcal{R}_2(\underline{\mathbf{curl}}(\widehat{\boldsymbol{\xi}}))| &\leq \widehat{C}_2 \left\{ \sum_{K \in \mathcal{T}_h} h_K^2 \|\mathbf{rot}(\mathbf{D}_h + \boldsymbol{\gamma}_h)\|_{0,K}^2 + \sum_{e \in \mathcal{E}_h(\Omega)} h_e \|\llbracket (\mathbf{D}_h + \boldsymbol{\gamma}_h) \mathbf{s} \rrbracket\|_{0,e}^2 \right. \\ &\quad \left. + \sum_{e \in \mathcal{E}_h(\Gamma)} h_e \|\nabla \mathbf{u}_D \mathbf{s} - (\mathbf{D}_h + \boldsymbol{\gamma}_h) \mathbf{s}\|_{0,e}^2 \right\}^{1/2} \|\boldsymbol{\tau}\|_{\mathbf{div}_{4/3};\Omega}. \end{aligned} \quad (3.37)$$

Finally, it is easy to see that (3.28), (3.29), (3.35), and (3.37) give (3.34), which ends the proof.  $\square$

We end this section by stressing that the reliability estimate (3.11) (cf. Theorem 3.1) follows by bounding each one of the terms  $\|\mathcal{R}_1\|_{\mathcal{H}'_1}$ ,  $\|\mathcal{R}_2\|_{\mathcal{H}'_2}$ , and  $\|\mathcal{R}_3\|_{\mathcal{Q}'}$ , in Lemma 3.2 by the corresponding upper bounds derived in Lemmas 3.3 and 3.4, and considering the definition of the global estimator  $\Theta$  (cf. (3.1)).

## 3.2 Efficiency

We now aim to establish the efficiency estimate of  $\Theta$  (cf. (3.1)). For this purpose, we will make extensive use of the notations and results from Appendix B, and the original system of equations given by (2.8), which is recovered from the mixed continuous formulation (2.11) by choosing suitable test functions and integrating by parts backwardly the corresponding equations. The following theorem is the main result of this section.

**Theorem 3.5.** *There exists a positive constant  $C_{\text{eff}}$ , independent of  $h$ , such that*

$$C_{\text{eff}} \Theta + \mathbf{h.o.t} \leq \|\vec{\mathbf{D}} - \vec{\mathbf{D}}_h\|_{\mathcal{H}} + \|p - p_h\|_{0,\Omega}, \quad (3.38)$$

where  $\mathbf{h.o.t}$  stands eventually for one or several terms of higher order.

Throughout this section we assume, without loss of generality, that  $\mathbf{u}_D$  is piecewise polynomial. Otherwise, if it is not, but it is sufficiently smooth, one proceeds similarly to [17, Section 6.2], so that higher order terms given by the error arising from a suitable polynomial approximation of this function appear in (3.38). This possibility explains the expression  $\mathbf{h.o.t}$  in (3.38).

We begin deriving the efficiency estimate (3.38) by first addressing  $\Theta_{1,K}$  and the first two terms of  $\Theta_{2,K}$  (cf. (3.2), (3.3)).

**Lemma 3.6.** *For each  $K \in \mathcal{T}_h$  there hold*

$$\|\mathbf{f} + \mathbf{div}(\boldsymbol{\sigma}_h)\|_{0,4/3;K} \leq \|\mathbf{div}(\boldsymbol{\sigma} - \boldsymbol{\sigma}_h)\|_{0,4/3;K} \quad (3.39)$$

$$\text{and } \|\boldsymbol{\sigma}_h - \boldsymbol{\sigma}_h^t\|_{0,K} \leq 2 \|\boldsymbol{\sigma} - \boldsymbol{\sigma}_h\|_{0,K}. \quad (3.40)$$

*In addition, there exists a positive constant  $C$ , independent of  $h$ , such that*

$$\begin{aligned} & \|\eta(p_h, |\mathbf{D}_h|) \mathbf{D}_h - \boldsymbol{\sigma}_h^d - \rho(\mathbf{u}_h \otimes \mathbf{u}_h)^d\|_{0,K} \\ & \leq C \left\{ \|\mathbf{D} - \mathbf{D}_h\|_{0,K} + \|\boldsymbol{\sigma} - \boldsymbol{\sigma}_h\|_{0,K} + \|\mathbf{u} - \mathbf{u}_h\|_{0,4;K} + \|p - p_h\|_{0,K} \right\}. \end{aligned} \quad (3.41)$$

*Proof.* First, in order to show (3.39) and (3.40), it suffices to recall that  $\mathbf{f} = -\mathbf{div}(\boldsymbol{\sigma})$  and  $\boldsymbol{\sigma} = \boldsymbol{\sigma}^t$  in  $\Omega$  (cf. (2.8)). In turn, for the proof of (3.41), we first use the identity  $\eta(p, |\mathbf{D}|) \mathbf{D} - \boldsymbol{\sigma}^d - \rho(\mathbf{u} \otimes \mathbf{u})^d = \mathbf{0}$  in  $\Omega$  (cf. (2.8)) and triangle inequality, to deduce

$$\begin{aligned} & \|\eta(p_h, |\mathbf{D}_h|) \mathbf{D}_h - \boldsymbol{\sigma}_h^d - \rho(\mathbf{u}_h \otimes \mathbf{u}_h)^d\|_{0,K} \\ & \leq \|\eta(p, |\mathbf{D}|) \mathbf{D} - \eta(p_h, |\mathbf{D}_h|) \mathbf{D}_h\|_{0,K} + \|\boldsymbol{\sigma} - \boldsymbol{\sigma}_h\|_{0,K} + \rho \|\mathbf{u} \otimes \mathbf{u} - \mathbf{u}_h \otimes \mathbf{u}_h\|_{0,K}, \end{aligned} \quad (3.42)$$

where, adding and subtracting  $\eta(p, |\mathbf{D}_h|) \mathbf{D}_h$  in the first term on the right-hand side of (3.42), and using the Lipschitz continuity estimates [12, eqs. (4.8) and (4.11)], we find that there exists positive constants  $L_{\mathcal{A}}, L_{\eta}$ , such that

$$\begin{aligned} & \|\eta(p, |\mathbf{D}|) \mathbf{D} - \eta(p_h, |\mathbf{D}_h|) \mathbf{D}_h\|_{0,K} \\ & \leq \|\eta(p, |\mathbf{D}|) \mathbf{D} - \eta(p, |\mathbf{D}_h|) \mathbf{D}_h\|_{0,K} + \|\{\eta(p, |\mathbf{D}_h|) - \eta(p_h, |\mathbf{D}_h|)\} \mathbf{D}_h\|_{0,K} \\ & \leq L_{\mathcal{A}} \|\mathbf{D} - \mathbf{D}_h\|_{0,K} + L_{\eta} \|p - p_h\|_{0,K}. \end{aligned} \quad (3.43)$$

In turn, proceeding as in (3.23) in combination with the fact that  $\|\mathbf{u}\|_{0,4;K}$  and  $\|\mathbf{u}_h\|_{0,4;K}$  are bounded by  $\|\mathbf{u}\|_{0,4;\Omega}$  and  $\|\mathbf{u}_h\|_{0,4;\Omega}$ , respectively, with  $\mathbf{u} \in \mathbf{W}(\delta)$  and  $\mathbf{u}_h \in \mathbf{W}(\delta_d)$ , there holds

$$\begin{aligned} & \|\mathbf{u} \otimes \mathbf{u} - \mathbf{u}_h \otimes \mathbf{u}_h\|_{0,K} \leq n^{1/2} (\|\mathbf{u}\|_{0,4;K} + \|\mathbf{u}_h\|_{0,4;K}) \|\mathbf{u} - \mathbf{u}_h\|_{0,4;K} \\ & \leq n^{1/2} (\|\mathbf{u}\|_{0,4;\Omega} + \|\mathbf{u}_h\|_{0,4;\Omega}) \|\mathbf{u} - \mathbf{u}_h\|_{0,4;K} \leq n^{1/2} (\delta + \delta_d) \|\mathbf{u} - \mathbf{u}_h\|_{0,4;K}. \end{aligned} \quad (3.44)$$

Finally, replacing back (3.43) and (3.44) into (3.42) we obtain (3.41) and conclude the proof.  $\square$

We remark that the local efficiency estimates for the remaining terms in the definition of  $\Theta$  (cf. (3.1)) have already been established in the literature. These estimates are derived using the localization technique based on triangle-bubble and edge-bubble functions (cf. (B.1) and Lemma B.1), together with the local inverse inequality (cf. (B.2)) and the discrete trace inequality (cf. (B.3)). For completeness, we state the following result.

**Lemma 3.7.** *There exist positive constants  $C_i$ ,  $i \in \{1, \dots, 5\}$ , all independent of  $h$ , such that*

- a)  $h_K^4 \|\nabla \mathbf{u}_h - (\mathbf{D}_h + \boldsymbol{\gamma}_h)\|_{0,4;K}^4 \leq C_1 \left\{ \|\mathbf{u} - \mathbf{u}_h\|_{0,4;K}^4 + h_K^2 \|\mathbf{D} - \mathbf{D}_h\|_{0,K}^4 + h_K^2 \|\boldsymbol{\gamma} - \boldsymbol{\gamma}_h\|_{0,K}^4 \right\} \quad \forall K \in \mathcal{T}_h,$
- b)  $h_e \|\mathbf{u}_D - \mathbf{u}_h\|_{0,4;e}^4 \leq C_2 \left\{ \|\mathbf{u} - \mathbf{u}_h\|_{0,4;K_e}^4 + h_{K_e}^2 \|\mathbf{D} - \mathbf{D}_h\|_{0,K_e}^4 + h_{K_e}^2 \|\boldsymbol{\gamma} - \boldsymbol{\gamma}_h\|_{0,K_e}^4 \right\} \quad \forall e \in \mathcal{E}_h(\Gamma),$
- c)  $h_K^2 \|\mathbf{rot}(\mathbf{D}_h + \boldsymbol{\gamma}_h)\|_{0,K}^2 \leq C_3 \left\{ \|\mathbf{D} - \mathbf{D}_h\|_{0,K}^2 + \|\boldsymbol{\gamma} - \boldsymbol{\gamma}_h\|_{0,K}^2 \right\} \quad \forall K \in \mathcal{T}_h,$

$$\text{d) } h_e \left\| [(\mathbf{D}_h + \gamma_h)\mathbf{s}] \right\|_{0,e}^2 \leq C_4 \left\{ \|\mathbf{D} - \mathbf{D}_h\|_{0,\omega_e}^2 + \|\gamma - \gamma_h\|_{0,\omega_e}^2 \right\} \quad \forall e \in \mathcal{E}_h(\Omega),$$

$$\text{e) } h_e \left\| \nabla \mathbf{u}_D \mathbf{s} - (\mathbf{D}_h + \gamma_h)\mathbf{s} \right\|_{0,e}^2 \leq C_5 \left\{ \|\mathbf{D} - \mathbf{D}_h\|_{0,K_e}^2 + \|\gamma - \gamma_h\|_{0,K_e}^2 \right\} \quad \forall e \in \mathcal{E}_h(\Gamma),$$

where  $K_e$  is the triangle of  $\mathcal{T}_h$  having  $e$  as an edge, whereas  $\omega_e$  denotes the union of the two elements of  $\mathcal{T}_h$  sharing the edge  $e$ .

*Proof.* The estimate a) follows directly from the proof of [28, Lemma 3.15], replacing  $\mathbf{t}_h$  therein with  $\mathbf{D}_h + \gamma_h$ , while b) is given in [28, Lemma 3.16]. For c) and d), we refer to [6, Lemmas 4.3 and 4.4]. Finally, the proof of e) follows the same arguments as those in [29, Lemma 4.15].  $\square$

We conclude this section by noting that the proof of (3.38) (cf. Theorem 3.5) follows directly from Lemmas 3.6 and 3.7 and summing the local efficiency estimates over all  $K \in \mathcal{T}_h$ . Further details are omitted.

## 4 Numerical results

This section serves to illustrate the performance and accuracy of the proposed mixed finite element scheme (2.21) along with the reliability and efficiency properties of the *a posteriori* error estimator  $\Theta$  (cf. (3.1)) derived in Section 3. In what follows, we refer to the corresponding sets of finite element subspaces generated by  $\ell = \{0, 1\}$  as simply PEERS $_\ell$  and AFW $_\ell$  based discretizations (cf. (2.19), (2.20)). The numerical methods have been implemented using the open source finite element library FEniCS [5]. Regarding the implementation of the Newton-type iterative method associated with (2.21) (see [12, steps (1)-(3) in Section 7] for details), the iterations are terminated once the relative error of the entire coefficient vectors between two consecutive iterates, namely  $\mathbf{coeff}^m$  and  $\mathbf{coeff}^{m+1}$ , is sufficiently small, that is,

$$\frac{\|\mathbf{coeff}^{m+1} - \mathbf{coeff}^m\|_{\text{DoF}}}{\|\mathbf{coeff}^{m+1}\|_{\text{DoF}}} \leq \text{tol},$$

where  $\|\cdot\|_{\text{DoF}}$  stands for the usual Euclidean norm in  $\mathbb{R}^{\text{DoF}}$  with DoF denoting the total number of degrees of freedom defining the finite element subspaces  $\mathcal{H}_{1,h}$ ,  $\tilde{\mathcal{H}}_{2,h}$ ,  $\mathcal{Q}_{1,h}$ , and  $\mathcal{Q}_{2,h}$  (cf. (2.19), (2.20)), and  $\text{tol}$  is a fixed tolerance chosen as  $\text{tol} = 1\text{E} - 06$ .

The global error and the effectivity index associated to the global estimator  $\Theta$  (cf. (3.1)) are denoted, respectively, by

$$\mathbf{e}(\vec{\mathbf{t}}) := \mathbf{e}(\mathbf{D}) + \mathbf{e}(\boldsymbol{\sigma}) + \mathbf{e}(\mathbf{u}) + \mathbf{e}(\gamma) + \mathbf{e}(p) \quad \text{and} \quad \text{eff}(\Theta) := \frac{\mathbf{e}(\vec{\mathbf{t}})}{\Theta},$$

where

$$\begin{aligned} \mathbf{e}(\mathbf{D}) &:= \|\mathbf{D} - \mathbf{D}_h\|_{0,\Omega}, & \mathbf{e}(\boldsymbol{\sigma}) &:= \|\boldsymbol{\sigma} - \boldsymbol{\sigma}_h\|_{\text{div}_{4/3};\Omega}, & \mathbf{e}(\mathbf{u}) &:= \|\mathbf{u} - \mathbf{u}_h\|_{0,4;\Omega}, \\ \mathbf{e}(\gamma) &:= \|\gamma - \gamma_h\|_{0,\Omega}, & \text{and } \mathbf{e}(p) &:= \|p - p_h\|_{0,\Omega}. \end{aligned}$$

Moreover, using the fact that  $\text{DoF}^{-1/n} \cong h$ , the respective experimental rates of convergence are computed as

$$r(\diamond) := -n \frac{\log(\mathbf{e}(\diamond)/\widehat{\mathbf{e}}(\diamond))}{\log(\text{DoF}/\widehat{\text{DoF}})} \quad \text{for each } \diamond \in \{\mathbf{D}, \boldsymbol{\sigma}, \mathbf{u}, \gamma, p, \vec{\mathbf{t}}\},$$

where DoF and  $\widehat{\text{DoF}}$  denote the total degrees of freedom associated to two consecutive triangulations with errors  $\mathbf{e}(\diamond)$  and  $\widehat{\mathbf{e}}(\diamond)$ , respectively. We stress that, for the sake of simplicity and clarity of

presentation, in the examples considered below we only report errors and rates of convergence for the most physically relevant unknowns, namely  $\boldsymbol{\sigma}$ ,  $\mathbf{u}$ ,  $p$ , and  $\vec{\mathbf{t}} = (\vec{\mathbf{D}}, p)$ . We recall that the reliability and efficiency of the global estimator  $\Theta$  (cf. (3.11), (3.38)) are with respect to the full error in  $\vec{\mathbf{t}}$ , and therefore we are particularly interested in the behavior of this error.

The examples to be considered in this section are described next, for which we consider the regularized viscosity  $\eta(\varrho, \omega)$  defined by (2.3). In the first three examples, for the sake of simplicity, we take  $\mu_s = 0.1$ ,  $\mu_d = 1$ ,  $I_0 = 1$ ,  $d = 1$  and  $\rho = 1$ . In addition, it is easy to see for these examples that the boundary data  $\mathbf{u}_D := \mathbf{u}|_\Gamma$  satisfy the required regularity  $\mathbf{u}_D \in \mathbf{H}^1(\Gamma)$  since the given exact solutions  $\mathbf{u}$  are sufficiently regular. In turn, the null mean value of  $\text{tr}(\boldsymbol{\sigma}_h)$  over  $\Omega$  is fixed via a real Lagrange multiplier strategy.

Example 1 is used to corroborate the reliability and efficiency of the *a posteriori* error estimator  $\Theta$ , whereas Examples 2, 3 and 4 are utilized to illustrate the behavior of the associated adaptive algorithm in 2D and 3D domains with and without manufactured solution, respectively, which applies the following procedure from [39]:

- (1) Start with a coarse mesh  $\mathcal{T}_h$  of  $\bar{\Omega}$ .
- (2) Solve the Newton iterative method associated with (2.21) on the current mesh.
- (3) Compute the local indicator  $\Theta_K$  for each  $K \in \mathcal{T}_h$ , where

$$\Theta_K := \Theta_{1,K} + \Theta_{2,K} + \Theta_{3,K} \quad (\text{cf. (3.2), (3.3), (3.4)}).$$

- (4) Check the stopping criterion and decide whether to finish or go to the next step.
- (5) Use Plaza and Carey's algorithm [36] to refine each  $K' \in \mathcal{T}_h$  satisfying

$$\Theta_{K'} \geq C_{\text{PC}} \max \left\{ \Theta_K : K \in \mathcal{T}_h \right\} \text{ for some } C_{\text{PC}} \in (0, 1).$$

- (6) Define the resulting mesh as the current mesh, and go to step (2).

In particular, in the 2D Examples 2 and 4 below, we set  $C_{\text{PC}} = \{0.25, 0.1\}$  for  $\ell = \{0, 1\}$ , respectively, while in the 3D Example 3, we set  $C_{\text{PC}} = 0.5$ .

### Example 1: Accuracy assessment with a smooth solution in a square domain

We first focus on the accuracy of the mixed methods and the properties of the *a posteriori* error estimator through the effectivity index  $\text{eff}(\Theta)$  under a quasi-uniform refinement strategy. We consider the square domain  $\Omega := (0, 1)^2$  and set the regularization parameter to  $\varepsilon = 1\text{E} - 08$ . The data  $\mathbf{f}$  and  $\mathbf{u}_D$  are adjusted so that a manufactured solution of (2.8) is given by the following smooth functions

$$\mathbf{u}(\mathbf{x}) = \begin{pmatrix} \sin(x_1) \cos(x_2) \\ -\cos(x_1) \sin(x_2) \end{pmatrix} \quad \text{and} \quad p(\mathbf{x}) = \exp(x_1 + x_2),$$

where  $p \in L_\kappa^2(\Omega)$ , with  $\kappa = (\exp(1) - 1)^2$ . Tables 4.1 and 4.2 shows the convergence history for a sequence of quasi-uniform mesh refinements for both PEERS $_\ell$  and AFW $_\ell$ -based discretizations, corresponding to  $\ell = 0$  and  $\ell = 1$ , respectively. The results are consistent with the theoretical bounds established in [12, Theorem 6.2]. In addition, we compute the global *a posteriori* error indicator  $\Theta$  (cf. (3.1)) and assess its reliability and efficiency through the effectivity index. We observe that the estimator remains uniformly bounded throughout the refinement process.

PEERS $_{\ell}$ -based discretization with $\ell = 0$ and quasi-uniform refinement												
DoF	$h$	it	$e(\boldsymbol{\sigma})$	$r(\boldsymbol{\sigma})$	$e(\mathbf{u})$	$r(\mathbf{u})$	$e(p)$	$r(p)$	$e(\vec{\mathbf{t}})$	$r(\vec{\mathbf{t}})$	$\Theta$	eff( $\Theta$ )
3314	0.177	14	5.5e-01	–	3.7e-02	–	2.0e-01	–	1.0e-00	–	1.1e-00	0.911
16634	0.079	12	2.4e-01	1.05	1.6e-02	1.06	7.8e-02	1.13	4.3e-01	1.06	5.3e-01	0.827
29522	0.059	12	1.8e-01	1.03	1.2e-02	1.03	5.8e-02	1.08	3.2e-01	1.04	4.0e-01	0.812
73874	0.037	11	1.1e-01	1.02	7.4e-03	1.01	3.6e-02	1.05	2.0e-01	1.03	2.5e-01	0.797
209282	0.022	9	6.5e-02	1.01	4.4e-03	1.01	2.1e-02	1.02	1.2e-01	1.02	1.5e-01	0.787
510602	0.014	8	4.2e-02	1.01	2.8e-03	1.00	1.3e-02	1.01	7.5e-02	1.01	9.6e-02	0.782

AFW $_{\ell}$ -based discretization with $\ell = 0$ and quasi-uniform refinement												
DoF	$h$	it	$e(\boldsymbol{\sigma})$	$r(\boldsymbol{\sigma})$	$e(\mathbf{u})$	$r(\mathbf{u})$	$e(p)$	$r(p)$	$e(\vec{\mathbf{t}})$	$r(\vec{\mathbf{t}})$	$\Theta$	eff( $\Theta$ )
2369	0.177	14	2.8e-01	–	3.5e-02	–	1.6e-01	–	5.4e-01	–	5.4e-01	0.995
11809	0.079	11	1.2e-01	1.01	1.6e-02	1.01	7.3e-02	1.01	2.4e-01	1.01	2.4e-01	1.003
20929	0.059	10	9.3e-02	1.01	1.2e-02	1.01	5.5e-02	1.01	1.8e-01	1.01	1.8e-01	1.004
52289	0.037	9	5.9e-02	1.00	7.3e-03	1.00	3.4e-02	1.00	1.1e-01	1.00	1.1e-01	1.005
147969	0.022	7	3.5e-02	1.00	4.4e-03	1.00	2.0e-02	1.00	6.7e-02	1.00	6.7e-02	1.005
360801	0.014	6	2.2e-02	1.00	2.8e-03	1.00	1.3e-02	1.00	4.3e-02	1.00	4.3e-02	1.005

Table 4.1: [Example 1,  $\ell = 0$ ] Number of degrees of freedom, meshsizes, Newton iteration count, errors, rates of convergence, global estimator, and effectivity index for the mixed approximations.

PEERS $_{\ell}$ -based discretization with $\ell = 1$ and quasi-uniform refinement												
DoF	$h$	it	$e(\boldsymbol{\sigma})$	$r(\boldsymbol{\sigma})$	$e(\mathbf{u})$	$r(\mathbf{u})$	$e(p)$	$r(p)$	$e(\vec{\mathbf{t}})$	$r(\vec{\mathbf{t}})$	$\Theta$	eff( $\Theta$ )
7010	0.177	10	1.2e-02	–	1.2e-03	–	4.5e-03	–	2.6e-02	–	4.6e-02	0.559
35210	0.079	7	2.4e-03	1.99	2.3e-04	2.01	8.9e-04	2.02	5.5e-03	1.93	9.5e-03	0.572
62498	0.059	7	1.3e-03	1.99	1.3e-04	2.01	5.0e-04	2.00	3.1e-03	1.96	5.4e-03	0.575
156410	0.037	6	5.4e-04	1.99	5.1e-05	2.00	2.0e-05	2.00	1.3e-03	1.97	2.2e-03	0.579
443138	0.022	4	1.9e-04	1.99	1.8e-05	2.00	7.0e-05	2.00	4.5e-04	1.98	7.7e-04	0.581
1081202	0.014	4	7.8e-05	2.00	7.3e-06	2.00	2.9e-05	2.00	1.9e-04	1.99	3.2e-04	0.583

AFW $_{\ell}$ -based discretization with $\ell = 1$ and quasi-uniform refinement												
DoF	$h$	it	$e(\boldsymbol{\sigma})$	$r(\boldsymbol{\sigma})$	$e(\mathbf{u})$	$r(\mathbf{u})$	$e(p)$	$r(p)$	$e(\vec{\mathbf{t}})$	$r(\vec{\mathbf{t}})$	$\Theta$	eff( $\Theta$ )
5473	0.177	7	6.1e-03	–	1.2e-03	–	4.3e-03	–	1.3e-02	–	2.1e-02	0.600
27433	0.079	5	1.2e-03	2.02	2.3e-04	2.01	8.6e-04	2.01	2.5e-03	2.02	4.3e-03	0.591
48673	0.059	5	6.7e-04	2.01	1.3e-04	2.01	4.8e-04	2.01	1.4e-03	2.01	2.4e-03	0.590
121753	0.037	4	2.7e-04	2.01	5.1e-05	2.01	1.9e-04	2.01	5.7e-04	2.01	9.6e-04	0.587
344833	0.022	3	9.4e-05	2.01	1.8e-05	2.00	6.8e-05	2.00	2.0e-04	2.01	3.4e-04	0.585
841201	0.014	3	3.8e-05	2.00	7.3e-06	2.00	2.8e-05	2.00	8.2e-05	2.00	1.4e-04	0.585

Table 4.2: [Example 1,  $\ell = 1$ ] Number of degrees of freedom, meshsizes, Newton iteration count, errors, rates of convergence, global estimator, and effectivity index for the mixed approximations.

## Example 2: Adaptivity in a 2D L-shaped domain

The second example is aimed at testing the features of adaptive mesh refinement after the *a posteriori* error estimator  $\Theta$  (cf. (3.1)). We consider a 2D L-shaped domain  $\Omega := (0, 1)^2 \setminus (0.5, 1)^2$  and the regularization parameter as  $\varepsilon = 1\text{E} - 08$ . The data  $\mathbf{f}$  and  $\mathbf{u}_D$  are chosen so that the exact solution is given by

$$\mathbf{u}(\mathbf{x}) = \begin{pmatrix} \sin(\pi x_1) \cos(\pi x_2) + x_2 \\ -\cos(\pi x_1) \sin(\pi x_2) + x_1 \end{pmatrix} \quad \text{and} \quad p(\mathbf{x}) = 18 - 10 \exp\left(\frac{-0.001}{r(\mathbf{x})}\right),$$

with  $r(\mathbf{x}) := (x_1 - 0.51)^2 + (x_2 - 0.51)^2$ . Notice that the pressure field exhibits high gradients near the vertex  $(0.5, 0.5)$ . Tables 4.3 and 4.4, together with Figure 4.1, summarize the convergence behavior of the mixed methods applied to a sequence of quasi-uniform and adaptively refined triangulations of the domain. Suboptimal convergence rates are observed in the quasi-uniform case. In contrast, adaptive refinement guided by the *a posteriori* error indicator  $\Theta$  leads to optimal rates and stable effectivity indices for both  $\text{PEERS}_\ell$  and  $\text{AFW}_\ell$ -based discretizations with  $\ell = \{0, 1\}$ . The adaptive strategy significantly enhances the efficiency of the method, enabling high-quality approximations at reduced computational cost. For  $\ell = 0$ , solutions with improved accuracy in terms of  $e(\vec{\mathbf{t}})$  are obtained using approximately 60% of the degrees of freedom required by the final quasi-uniform mesh. This reduction is significant, especially considering the challenges posed by the nonlinearities involved in the model. This efficiency is further enhanced for  $\ell = 1$ , where accurate solutions are obtained using only approximately 10% of the degrees of freedom, highlighting the substantial advantage of the adaptive approach in this case. Figure 4.2 displays the initial mesh and some approximate solutions computed with the adaptive  $\text{PEERS}_1$ -based method, using  $\Theta$ , on a mesh with 706,301 degrees of freedom and 13,061 triangles. These results confirm that the pressure exhibits strong variations in the contraction region. Additionally, Figure 4.3 shows examples of adapted meshes for the mixed methods when  $\ell = 1$ . As expected, the refinement is concentrated near the reentrant corner of the 2D L-shaped domain, revealing the indicator's ability to effectively localize the singularity.

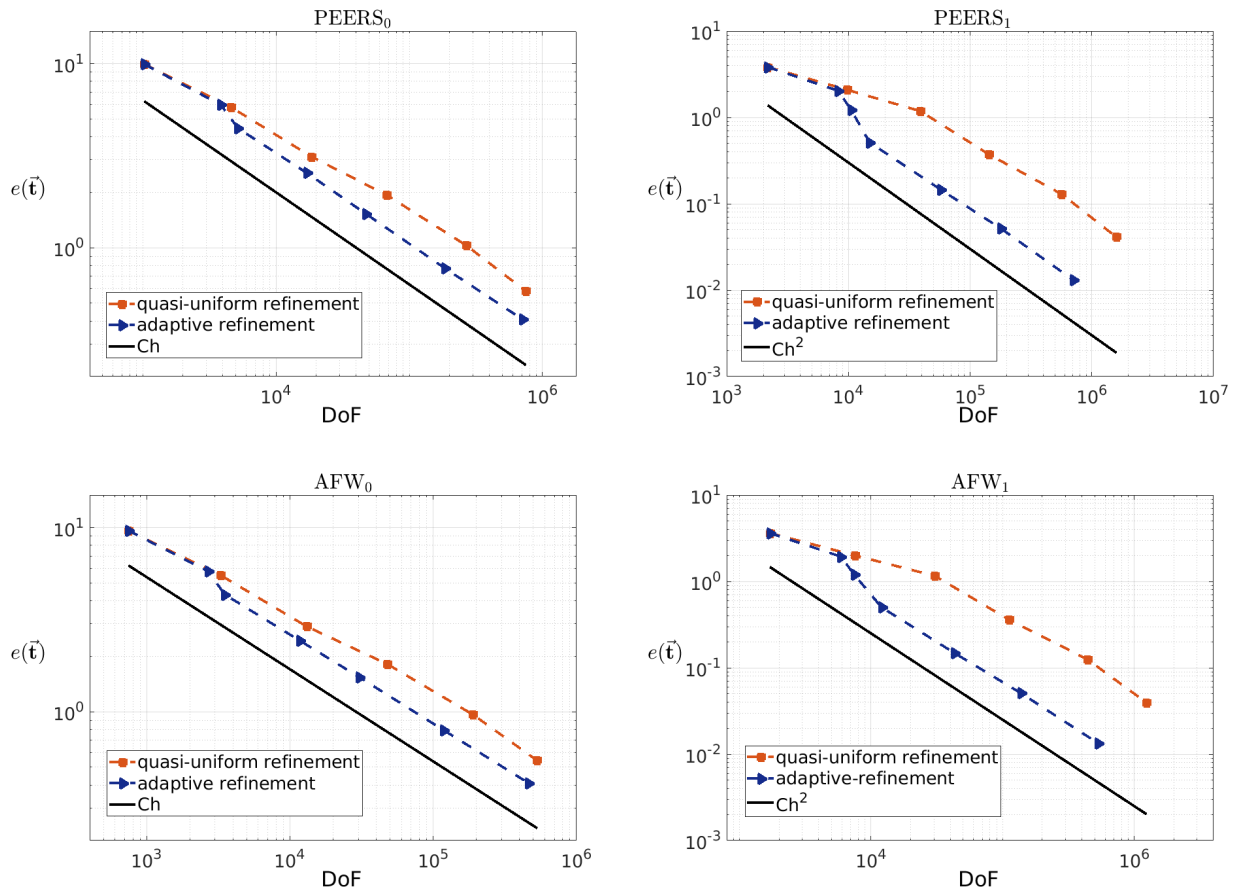


Figure 4.1: [Example 2] Log-log plot of  $e(\vec{\mathbf{t}})$  vs. DoF for quasi-uniform/adaptive refinements for  $\text{PEERS}_\ell$  and  $\text{AFW}_\ell$ -based discretizations with  $\ell = \{0, 1\}$  (top and bottom plots, respectively).

PEERS $_{\ell}$ -based discretization with $\ell = 0$ and quasi-uniform refinement												
DoF	$h$	it	$e(\boldsymbol{\sigma})$	$r(\boldsymbol{\sigma})$	$e(\mathbf{u})$	$r(\mathbf{u})$	$e(p)$	$r(p)$	$e(\vec{\mathbf{t}})$	$r(\vec{\mathbf{t}})$	$\Theta$	eff( $\Theta$ )
1028	0.280	15	8.0e-00	–	1.9e-01	–	7.0e-01	–	9.9e-00	–	9.8e-00	1.009
4601	0.141	18	4.9e-00	0.64	9.0e-02	0.97	3.4e-01	0.97	5.8e-00	0.72	5.7e-00	1.016
18491	0.071	15	2.7e-00	0.86	4.4e-02	1.04	1.8e-01	0.94	3.1e-00	0.89	3.1e-00	1.022
67811	0.038	13	1.7e-00	0.71	2.3e-02	0.99	9.8e-02	0.91	1.9e-00	0.74	1.9e-00	1.023
267785	0.019	12	9.2e-01	0.91	1.1e-02	1.01	5.0e-02	0.96	1.0e-00	0.92	1.0e-00	1.020
752408	0.011	11	5.2e-01	1.12	6.8e-03	1.00	2.9e-02	1.06	5.8e-01	1.11	5.7e-01	1.018

PEERS $_{\ell}$ -based discretization with $\ell = 0$ and adaptive refinement via $\Theta$											
DoF	it	$e(\boldsymbol{\sigma})$	$r(\boldsymbol{\sigma})$	$e(\mathbf{u})$	$r(\mathbf{u})$	$e(p)$	$r(p)$	$e(\vec{\mathbf{t}})$	$r(\vec{\mathbf{t}})$	$\Theta$	eff( $\Theta$ )
1028	15	8.0e-00	–	1.9e-01	–	7.0e-01	–	9.9e-00	–	9.8e-00	1.009
3857	17	5.1e-00	0.68	1.0e-01	0.90	3.6e-01	1.02	6.0e-00	0.77	6.0e-00	0.999
5189	17	3.7e-00	2.11	8.9e-02	0.92	2.7e-01	1.92	4.5e-00	1.98	4.5e-00	0.979
16997	14	2.2e-00	0.90	5.0e-02	0.98	1.4e-01	1.15	2.6e-00	0.94	2.6e-00	0.967
47183	14	1.3e-00	1.03	3.3e-02	0.82	8.6e-02	0.91	1.5e-00	1.00	1.6e-00	0.967
184580	13	6.6e-01	0.98	1.6e-02	1.03	4.2e-02	1.05	7.8e-01	1.00	8.1e-01	0.962
710489	12	3.5e-01	0.94	8.1e-03	1.03	2.2e-02	0.96	4.1e-01	0.95	4.2e-01	0.966

AFW $_{\ell}$ -based discretization with $\ell = 0$ and quasi-uniform refinement												
DoF	$h$	it	$e(\boldsymbol{\sigma})$	$r(\boldsymbol{\sigma})$	$e(\mathbf{u})$	$r(\mathbf{u})$	$e(p)$	$r(p)$	$e(\vec{\mathbf{t}})$	$r(\vec{\mathbf{t}})$	$\Theta$	eff( $\Theta$ )
745	0.280	19	7.9e-00	–	1.8e-01	–	8.0e-01	–	9.6e-00	–	8.7e-00	1.106
3285	0.141	19	4.7e-00	0.69	9.0e-02	0.96	3.3e-01	1.18	5.5e-00	0.75	5.2e-00	1.061
13117	0.071	18	2.5e-00	0.90	4.4e-02	1.04	1.5e-01	1.16	2.9e-00	0.93	2.8e-00	1.039
47997	0.038	17	1.6e-00	0.70	2.3e-02	0.99	8.1e-02	0.93	1.8e-00	0.73	1.8e-00	1.032
189285	0.019	17	8.7e-01	0.91	1.1e-02	1.01	4.2e-02	0.94	9.7e-01	0.92	9.4e-01	1.030
531593	0.011	16	4.9e-01	1.12	6.8e-03	1.00	2.4e-02	1.09	5.4e-01	1.11	5.3e-01	1.028

AFW $_{\ell}$ -based discretization with $\ell = 0$ and adaptive refinement via $\Theta$											
DoF	it	$e(\boldsymbol{\sigma})$	$r(\boldsymbol{\sigma})$	$e(\mathbf{u})$	$r(\mathbf{u})$	$e(p)$	$r(p)$	$e(\vec{\mathbf{t}})$	$r(\vec{\mathbf{t}})$	$\Theta$	eff( $\Theta$ )
745	19	7.9e-00	–	1.8e-01	–	8.0e-01	–	9.6e-00	–	8.7e-00	1.106
2685	19	4.9e-00	0.74	9.9e-02	0.95	3.6e-01	1.25	5.8e-00	0.80	5.4e-00	1.064
3517	19	3.6e-00	2.32	9.1e-02	0.63	2.4e-01	2.83	4.3e-00	2.16	4.1e-00	1.052
11729	18	2.1e-00	0.91	4.8e-02	1.07	1.0e-01	1.46	2.4e-00	0.96	2.4e-00	1.026
30457	18	1.3e-00	0.98	3.3e-02	0.76	5.7e-02	1.20	1.5e-00	0.96	1.5e-00	1.015
118453	17	6.8e-01	0.96	1.7e-02	1.03	2.9e-02	1.02	7.9e-01	0.97	7.8e-01	1.016
462749	15	3.5e-01	0.96	8.3e-03	1.02	1.5e-02	0.98	4.1e-01	0.97	4.0e-01	1.017

Table 4.3: [Example 2,  $\ell = 0$ ] Comparison of the mixed approximations with quasi-uniform and adaptive refinements for the  $\mu(I)$ -rheology model.

### Example 3: Adaptivity in a 3D L-shaped domain

Here, we replicate the Example 2 in a three-dimensional setting but now considering the 3D L-shaped domain  $\Omega = (0, 1) \times (0, 0.5) \times (0, 1) \setminus (0.5, 1) \times (0, 0.5) \times (0.5, 1)$ , the regularization parameter as  $\varepsilon = 1\text{E} - 06$ , and the manufactured exact solutions given by

$$\mathbf{u}(\mathbf{x}) = \begin{pmatrix} \sin(x_1) \cos(x_2) \cos(x_3) \\ -2 \cos(x_1) \sin(x_2) \cos(x_3) \\ \cos(x_1) \cos(x_2) \sin(x_3) \end{pmatrix} \quad \text{and} \quad p(\mathbf{x}) = 80 - 40 \exp\left(\frac{-0.0001}{r(\mathbf{x})}\right),$$

PEERS $_{\ell}$ -based discretization with $\ell = 1$ and quasi-uniform refinement												
DoF	$h$	it	$e(\boldsymbol{\sigma})$	$r(\boldsymbol{\sigma})$	$e(\mathbf{u})$	$r(\mathbf{u})$	$e(p)$	$r(p)$	$e(\bar{\mathbf{t}})$	$r(\bar{\mathbf{t}})$	$\Theta$	eff( $\Theta$ )
2171	0.280	16	3.4e-00	–	2.4e-02	–	2.4e-01	–	3.8e-00	–	3.9e-00	0.979
9734	0.141	14	1.9e-00	0.75	5.6e-03	1.95	9.1e-02	1.28	2.1e-00	0.80	2.1e-00	1.021
39143	0.071	12	1.1e-00	0.77	1.3e-03	2.13	3.2e-02	1.50	1.2e-00	0.82	1.2e-00	1.028
143573	0.038	9	3.5e-01	1.80	3.5e-04	1.99	1.3e-02	1.39	3.7e-01	1.78	3.6e-01	1.032
567023	0.019	7	1.2e-01	1.53	8.8e-05	2.00	4.1e-03	1.66	1.3e-01	1.54	1.3e-01	1.034
1593242	0.011	5	3.9e-02	2.22	3.1e-05	2.00	1.3e-03	2.28	4.1e-02	2.22	4.0e-02	1.029

PEERS $_{\ell}$ -based discretization with $\ell = 1$ and adaptive refinement via $\Theta$											
DoF	it	$e(\boldsymbol{\sigma})$	$r(\boldsymbol{\sigma})$	$e(\mathbf{u})$	$r(\mathbf{u})$	$e(p)$	$r(p)$	$e(\bar{\mathbf{t}})$	$r(\bar{\mathbf{t}})$	$\Theta$	eff( $\Theta$ )
2171	16	3.4e-00	–	2.4e-02	–	2.4e-01	–	3.8e-00	–	3.9e-00	0.979
8267	14	1.9e-00	0.90	6.3e-03	2.00	9.7e-02	1.32	2.0e-00	0.95	2.0e-00	1.024
10547	14	1.2e-00	4.04	6.2e-03	0.08	3.9e-02	7.56	1.2e-00	4.17	1.3e-00	0.965
14948	13	4.6e-01	5.25	5.4e-03	0.83	1.9e-02	4.17	5.1e-01	4.98	5.8e-01	0.880
57371	11	1.3e-01	1.87	1.4e-03	2.05	5.4e-03	1.85	1.5e-01	1.87	1.6e-01	0.891
179354	9	4.7e-02	1.80	3.6e-04	2.33	1.9e-03	1.87	5.2e-02	1.82	5.6e-02	0.918
706301	7	1.2e-02	2.00	9.1e-05	2.02	4.7e-04	2.01	1.3e-02	2.00	1.4e-02	0.916

AFW $_{\ell}$ -based discretization with $\ell = 1$ and quasi-uniform refinement												
DoF	$h$	it	$e(\boldsymbol{\sigma})$	$r(\boldsymbol{\sigma})$	$e(\mathbf{u})$	$r(\mathbf{u})$	$e(p)$	$r(p)$	$e(\bar{\mathbf{t}})$	$r(\bar{\mathbf{t}})$	$\Theta$	eff( $\Theta$ )
1702	0.280	15	3.3e-00	–	2.4e-02	–	2.3e-01	–	3.6e-00	–	3.5e-00	1.027
7597	0.141	13	1.9e-00	0.76	5.5e-03	1.95	9.0e-02	1.27	2.0e-00	0.81	1.9e-00	1.035
30490	0.071	11	1.1e-00	0.73	1.3e-03	2.12	3.1e-02	1.56	1.2e-00	0.77	1.1e-00	1.033
111760	0.038	8	3.5e-01	1.82	3.5e-04	1.99	1.3e-02	1.37	3.6e-01	1.80	3.5e-01	1.033
441202	0.019	6	1.2e-01	1.54	8.8e-05	2.01	4.0e-03	1.66	1.3e-01	1.54	1.2e-01	1.028
1239529	0.011	5	3.8e-02	2.23	3.1e-05	2.00	1.2e-03	2.30	3.9e-02	2.24	3.9e-02	1.020

AFW $_{\ell}$ -based discretization with $\ell = 1$ and adaptive refinement via $\Theta$											
DoF	it	$e(\boldsymbol{\sigma})$	$r(\boldsymbol{\sigma})$	$e(\mathbf{u})$	$r(\mathbf{u})$	$e(p)$	$r(p)$	$e(\bar{\mathbf{t}})$	$r(\bar{\mathbf{t}})$	$\Theta$	eff( $\Theta$ )
1702	15	3.3e-00	–	2.4e-02	–	2.3e-01	–	3.6e-00	–	3.5e-00	1.027
5893	14	1.8e-00	0.96	7.4e-03	1.88	9.5e-02	1.45	1.9e-00	1.01	1.9e-00	1.020
7456	13	1.1e-00	3.98	7.3e-03	0.04	3.4e-02	8.73	1.2e-00	4.10	1.2e-00	0.967
12022	13	4.7e-01	3.72	5.6e-03	1.19	1.3e-02	4.06	5.0e-01	3.65	5.4e-01	0.931
43087	11	1.4e-01	1.91	1.5e-03	2.09	4.1e-03	1.81	1.5e-01	1.91	1.6e-01	0.934
137791	9	4.7e-02	1.84	3.9e-04	2.28	1.5e-03	1.69	5.1e-02	1.84	5.3e-02	0.951
534541	6	1.2e-02	1.98	9.7e-05	2.04	4.1e-04	1.96	1.3e-02	1.98	1.4e-02	0.954

Table 4.4: [Example 2,  $\ell = 1$ ] Comparison of the mixed approximations with quasi-uniform and adaptive refinements for the  $\mu(I)$ -rheology model.

with  $r(\mathbf{x}) := (x_1 - 0.505)^2 + (x_3 - 0.505)^2$ . The convergence history for a set of quasi-uniform and adaptive mesh refinements using both PEERS $_0$  and AFW $_0$ -based discretizations is shown in Table 4.5, along with Figure 4.4. We observe a considerable increase in the number of degrees of freedom in the PEERS $_0$ -based scheme compared to the AFW $_0$  one. For this reason, and due to computational limitations, we report results for only four meshes in the case of the PEERS $_0$ -based discretization. This is mainly explained by the fact that the symmetric part of the velocity gradient is approximated using  $\mathbb{P}_3(\Omega)$  and  $\mathbb{P}_1(\Omega)$ , respectively. Nevertheless, in both cases we observe disturbed convergence under quasi-uniform refinement and optimal convergence rates when using adaptive refinement guided by the *a posteriori* error estimator  $\Theta$  (cf. (3.1)). The initial mesh and some approximate solutions

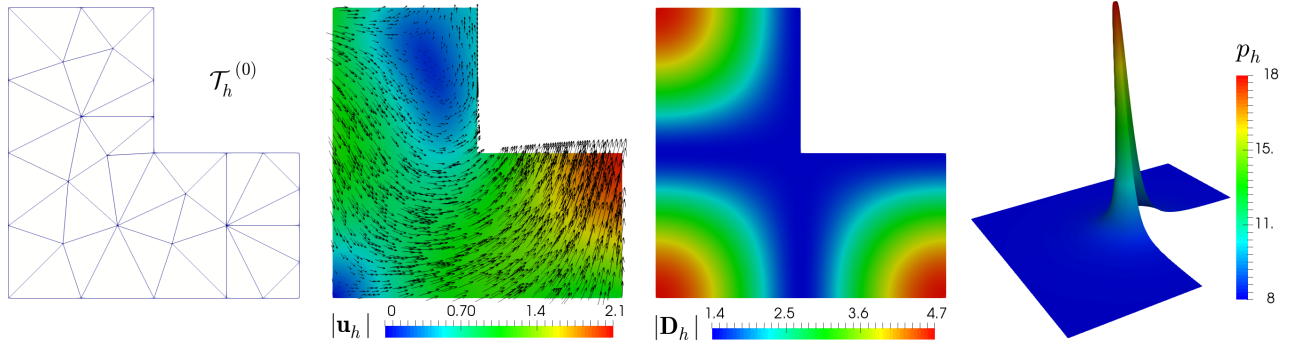


Figure 4.2: [Example 2] Initial mesh, computed magnitude of the velocity and symmetric part of the velocity gradient, and pressure field.

computed using the adaptive AFW<sub>0</sub>-based scheme (driven by  $\Theta$ ), with 775,808 degrees of freedom and 13,724 tetrahedra, are displayed in Figure 4.5. Snapshots of three meshes generated via  $\Theta$  are shown in Figure 4.6, where an incipient clustering of elements around the contraction region can be observed.

#### Example 4: Fluid flow through a 2D cavity with two circular obstacles

Inspired by [12, Example 3 in Section 7], we finally focus on studying the behavior of the regularized  $\mu(I)$ -rheology model for granular materials in fluid flow through a 2D cavity with two circular obstacles, without employing a manufactured solution. More precisely, we consider the domain  $\Omega = (0, 1)^2 \setminus \Omega_c$ , where

$$\Omega_c = \left\{ (x_1, x_2) : (x_1 - 1/2)^2 + (x_2 - 1/3)^2 < 0.1^2 \right\} \cup \left\{ (x_1, x_2) : (x_1 - 1/2)^2 + (x_2 - 2/3)^2 < 0.1^2 \right\},$$

with boundary  $\Gamma$ , whose part around the circles is given by  $\Gamma_c = \partial\Omega_c$ . The model parameters are chosen as  $\mu_s = 0.36$ ,  $\mu_d = 0.91$ ,  $I_0 = 0.73$ ,  $d = 0.05$ ,  $\rho = 2500$ , and the regularization factor is  $\varepsilon = 1\text{E} - 03$ . Notice that the relation between the diameter of the particles  $d$  and the width of the cavity is 1 : 20, whereas the radius of both circular obstacles is double that of  $d$ . The mean value of  $p$  is fixed as  $\kappa = 100$ , no presence of gravity is assumed, that is,  $\mathbf{f} = \mathbf{0}$ , and the boundaries conditions are

$$\mathbf{u} = (0.2x_2 - 0.1, 0)^t \quad \text{on } \Gamma \setminus \Gamma_c \quad \text{and} \quad \mathbf{u} = \mathbf{0} \quad \text{on } \Gamma_c.$$

In particular, we impose that flows cannot go in nor out through  $\Gamma_c$ , whereas at the top and bottom of the domain flows are faster in opposite direction. In Figure 4.7, we display the initial mesh, the computed magnitude of the velocity and symmetric part of the velocity gradient, and pressure field, which were built using the mixed PEERS<sub>0</sub>-based scheme on a mesh with 23,390 triangle elements (actually representing 597,375 DoF) obtained via  $\Theta$  (cf. (3.1)). Similarly to [12, Example 3 in Section 7], we observe higher velocities along the top and bottom boundaries, moving rightward and leftward, respectively, as anticipated. Additionally, a circulation phenomenon emerges near the lateral boundaries, driven by the fact that the fluid cannot enter or exit through the circular obstacles. Most of the variations in both the pressure field and the magnitude of the symmetric part of the velocity gradient tensor are concentrated around the circular obstacles. Notably, between the obstacles and in some central regions of the domain, the magnitude of the symmetric part of the velocity gradient is either zero or nearly so, indicating zones where the original viscosity  $\eta$  (cf. [12, eq. (2.9)]) becomes

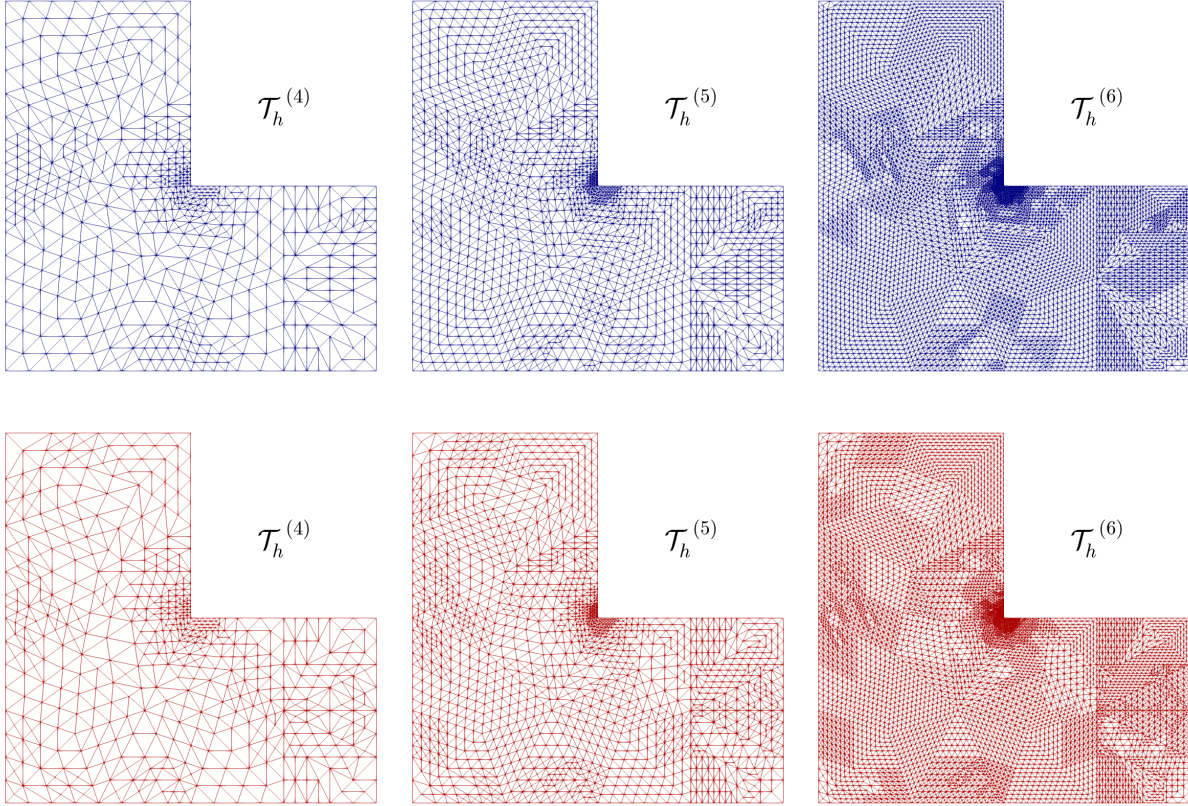


Figure 4.3: [Example 2] Three snapshots of adapted meshes according to the indicator  $\Theta$  for PEERS<sub>1</sub> and AFW<sub>1</sub>-based discretizations (top and bottom plots, respectively).

singular and the granular flow remains static. This behavior is consistent with the velocity field and is properly handled by the mixed formulations using the regularized viscosity (2.3). The results align with those reported in [12], now incorporating an adaptive mesh refinement strategy driven by the *a posteriori* error indicator  $\Theta$ . Snapshots of some of the adapted meshes are shown in Figure 4.8, where we can clearly observe refinement concentrated around the obstacles and in regions where the velocity gradient vanishes or is nearly zero. This confirms that the indicator  $\Theta$  successfully identifies both the singular zones and the areas with large solution variations, as intended.

## A Preliminaries for reliability

We begin by introducing useful notations to describe local information on elements and edges. For each  $K \in \mathcal{T}_h$ , let  $\mathcal{E}(K)$  denote its set of edges, and let  $\mathcal{E}_h$  be the set of all edges in  $\mathcal{T}_h$ , with corresponding diameters  $h_e$ . We further decompose  $\mathcal{E}_h$  as  $\mathcal{E}_h = \mathcal{E}_h(\Omega) \cup \mathcal{E}_h(\Gamma)$ , where  $\mathcal{E}_h(\Omega) := \{e \in \mathcal{E}_h : e \subseteq \Omega\}$  and  $\mathcal{E}_h(\Gamma) := \{e \in \mathcal{E}_h : e \subseteq \Gamma\}$ . For each  $e \in \mathcal{E}_h$ , we fix unit normal and tangential vectors, denoted by  $\boldsymbol{\nu}_e := (\nu_1, \nu_2)^t$  and  $\mathbf{s}_e := (-\nu_2, \nu_1)^t$ , respectively. When no ambiguity arises, we will simply write  $\boldsymbol{\nu}$  and  $\mathbf{s}$ . The usual jump operator  $[[\cdot]]$  across an internal edge  $e \in \mathcal{E}_h(\Omega)$  is defined for a piecewise continuous tensor valued function  $\boldsymbol{\zeta}$  as  $[[\boldsymbol{\zeta}]] := \boldsymbol{\zeta}|_K - \boldsymbol{\zeta}|_{K'}$ , where  $K$  and  $K'$  are the elements of  $\mathcal{T}_h$  sharing  $e$ . Finally, for a scalar field  $\phi$ , a vector field  $\mathbf{v} := (v_1, v_2)^t$ , and a matrix-valued field  $\boldsymbol{\tau} := (\tau_{ij})_{2 \times 2}$ , we

PEERS $_{\ell}$ -based discretization with $\ell = 0$ and quasi-uniform refinement												
DoF	$h$	it	$e(\boldsymbol{\sigma})$	$r(\boldsymbol{\sigma})$	$e(\mathbf{u})$	$r(\mathbf{u})$	$e(p)$	$r(p)$	$e(\vec{\mathbf{t}})$	$r(\vec{\mathbf{t}})$	$\Theta$	$\text{eff}(\Theta)$
32744	0.522	18	1.3e+01	–	9.8e-02	–	2.1e-00	–	1.6e+01	–	1.2e+01	1.271
296142	0.207	16	6.5e-00	0.97	4.1e-02	1.18	8.7e-01	1.19	7.5e-00	1.00	6.4e-00	1.181
605245	0.164	16	5.8e-00	0.49	3.2e-02	1.03	6.9e-01	0.98	6.6e-00	0.55	5.6e-00	1.168
1651385	0.114	16	5.2e-00	0.31	2.3e-02	1.03	4.9e-01	1.03	5.8e-00	0.39	5.0e-00	1.149

PEERS $_{\ell}$ -based discretization with $\ell = 0$ and adaptive refinement via $\Theta$											
DoF	it	$e(\boldsymbol{\sigma})$	$r(\boldsymbol{\sigma})$	$e(\mathbf{u})$	$r(\mathbf{u})$	$e(p)$	$r(p)$	$e(\vec{\mathbf{t}})$	$r(\vec{\mathbf{t}})$	$\Theta$	$\text{eff}(\Theta)$
32744	18	1.3e+01	–	9.8e-02	–	2.1e-00	–	1.6e+01	–	1.2e+01	1.271
106606	17	7.2e-00	1.55	7.4e-02	0.70	9.8e-01	1.90	8.4e-00	1.59	7.2e-00	1.157
374390	17	5.2e-00	0.78	6.2e-02	0.43	4.7e-01	1.78	5.8e-00	0.88	5.3e-00	1.084
935833	17	3.8e-00	1.05	4.1e-02	1.36	2.5e-01	2.08	4.1e-00	1.12	3.9e-00	1.061

AFW $_{\ell}$ -based discretization with $\ell = 0$ and quasi-uniform refinement												
DoF	$h$	it	$e(\boldsymbol{\sigma})$	$r(\boldsymbol{\sigma})$	$e(\mathbf{u})$	$r(\mathbf{u})$	$e(p)$	$r(p)$	$e(\vec{\mathbf{t}})$	$r(\vec{\mathbf{t}})$	$\Theta$	$\text{eff}(\Theta)$
10911	0.522	11	1.3e+01	–	9.8e-02	–	2.0e-00	–	1.5e+01	–	1.2e+01	1.267
94997	0.207	10	6.4e-00	1.00	4.1e-02	1.20	8.6e-01	1.20	7.3e-00	1.03	6.3e-00	1.173
193678	0.164	10	5.7e-00	0.51	3.2e-02	1.04	6.8e-01	1.00	6.4e-00	0.57	5.5e-00	1.154
525096	0.114	10	5.1e-00	0.34	2.3e-02	1.04	4.8e-01	1.03	5.6e-00	0.41	5.0e-00	1.126
1595337	0.079	10	4.4e-00	0.39	1.6e-02	1.04	3.3e-01	1.05	4.7e-00	0.44	4.3e-00	1.105

AFW $_{\ell}$ -based discretization with $\ell = 0$ and adaptive refinement via $\Theta$											
DoF	it	$e(\boldsymbol{\sigma})$	$r(\boldsymbol{\sigma})$	$e(\mathbf{u})$	$r(\mathbf{u})$	$e(p)$	$r(p)$	$e(\vec{\mathbf{t}})$	$r(\vec{\mathbf{t}})$	$\Theta$	$\text{eff}(\Theta)$
10911	11	1.3e+01	–	9.8e-02	–	2.0e-00	–	1.5e+01	–	1.2e+01	1.267
34300	11	7.0e-00	1.64	7.4e-02	0.72	9.7e-01	1.93	8.2e-00	1.66	7.2e-00	1.140
114721	11	5.0e-00	0.86	6.2e-02	0.44	4.6e-01	1.88	5.6e-00	0.96	5.3e-00	1.043
314569	10	3.6e-00	1.01	3.9e-02	1.41	2.3e-01	2.02	3.9e-00	1.09	3.8e-00	1.013
775808	10	2.6e-00	1.08	2.8e-02	1.14	1.5e-01	1.40	2.8e-00	1.10	2.8e-00	1.002

Table 4.5: [Example 3,  $\ell = 0$ ] Comparison of the mixed approximations with quasi-uniform and adaptive refinements for the  $\mu(I)$ -rheology model.

define:

$$\mathbf{curl}(\phi) := \left( \frac{\partial \phi}{\partial x_2}, -\frac{\partial \phi}{\partial x_1} \right)^t, \quad \mathbf{curl}(\mathbf{v}) := \begin{pmatrix} \mathbf{curl}(v_1)^t \\ \mathbf{curl}(v_2)^t \end{pmatrix},$$

$$\mathbf{rot}(\mathbf{v}) := \frac{\partial v_1}{\partial x_2} - \frac{\partial v_2}{\partial x_1}, \quad \text{and} \quad \mathbf{rot}(\boldsymbol{\tau}) := \begin{pmatrix} \mathbf{rot}(\tau_{11}, \tau_{12}) \\ \mathbf{rot}(\tau_{21}, \tau_{22}) \end{pmatrix},$$

where the derivatives involved are taken in the distributional sense.

Let us now recall the main properties of the Raviart–Thomas and Clément interpolation operators (cf. [22], [19]). We begin by defining, for each  $p \geq 2n/(n+2)$ , the spaces

$$\mathbf{W}_p(\Omega) := \left\{ \boldsymbol{\tau} \in \mathbf{H}(\mathbf{div}_p; \Omega) : \boldsymbol{\tau}|_K \in \mathbf{W}^{1,p}(K), \quad \forall K \in \mathcal{T}_h \right\}, \quad (\text{A.1})$$

and

$$\mathbf{RT}_{\ell}(\Omega) := \left\{ \boldsymbol{\tau} \in \mathbf{H}(\mathbf{div}_p; \Omega) : \boldsymbol{\tau}|_K \in \mathbf{RT}_{\ell}(K), \quad \forall K \in \mathcal{T}_h \right\}. \quad (\text{A.2})$$

In addition, we let  $\Pi_h^{\ell} : \mathbf{W}_p(\Omega) \rightarrow \mathbf{RT}_{\ell}(\Omega)$  be the Raviart–Thomas interpolation operator, which is

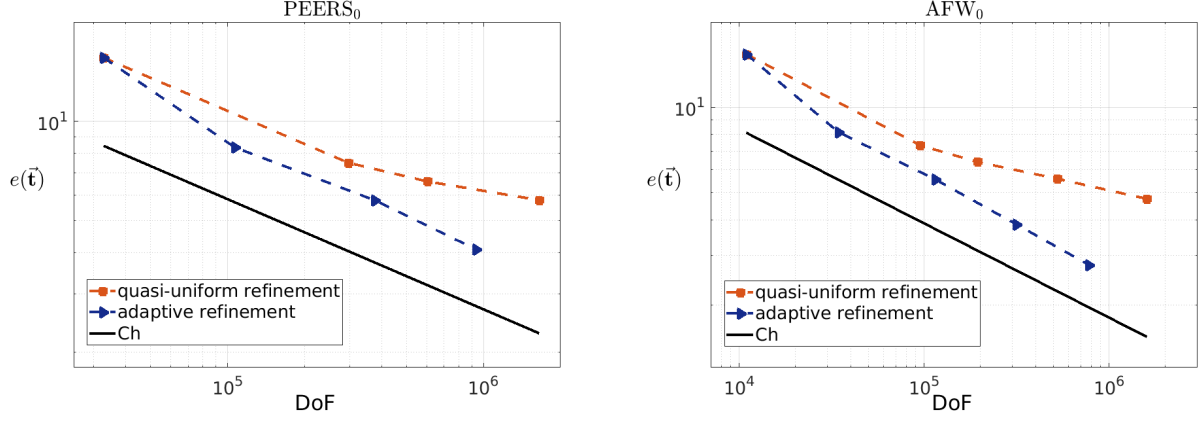


Figure 4.4: [Example 3] Log-log plot of  $e(\tilde{\mathbf{t}})$  vs. DoF for quasi-uniform/adaptive refinements for  $\text{PEERS}_0$  and  $\text{AFW}_0$ -based discretizations (left and right plots, respectively).

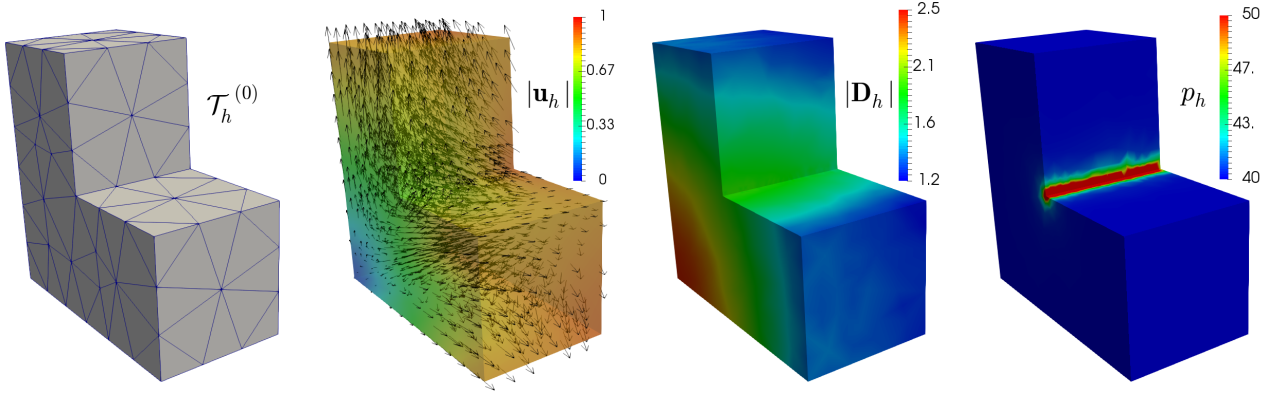


Figure 4.5: [Example 3] Initial mesh, computed magnitude of the velocity and symmetric part of the velocity gradient, and pressure field.

characterized for each  $\boldsymbol{\tau} \in \mathbf{W}_p(\Omega)$  by the identities (see, e.g. [22, Section 1.2.7])

$$\int_e \left( \Pi_h^\ell(\boldsymbol{\tau}) \cdot \boldsymbol{\nu} \right) \xi = \int_e (\boldsymbol{\tau} \cdot \boldsymbol{\nu}) \xi \quad \forall \xi \in \mathbf{P}_k(e), \quad \forall \text{ edge or face } e \text{ of } \mathcal{T}_h, \quad (\text{A.3})$$

when  $k \geq 0$ , and

$$\int_K \Pi_h^\ell(\boldsymbol{\tau}) \cdot \boldsymbol{\psi} = \int_K \boldsymbol{\tau} \cdot \boldsymbol{\psi} \quad \forall \boldsymbol{\psi} \in \mathbf{P}_{\ell-1}(K), \quad \forall K \in \mathcal{T}_h, \quad (\text{A.4})$$

when  $k \geq 1$ . In turn, given  $q > 1$  such that  $1/p + 1/q = 1$ , we let

$$\mathbf{P}_\ell(\Omega) := \left\{ v \in L^q(\Omega) : v|_K \in \mathbf{P}_\ell(K), \quad \forall K \in \mathcal{T}_h \right\}, \quad (\text{A.5})$$

and recall from [22, Lemma 1.41] that there holds

$$\text{div}(\Pi_h^\ell(\boldsymbol{\tau})) = \mathcal{P}_h^\ell(\text{div}(\boldsymbol{\tau})), \quad \forall \boldsymbol{\tau} \in \mathbf{W}_p(\Omega), \quad (\text{A.6})$$

where  $\mathcal{P}_h^\ell : L^2(\Omega) \rightarrow \mathbf{P}_\ell(\Omega)$  denotes the standard orthogonal projector with respect to the  $L^2(\Omega)$ -inner product. This operator satisfies the following error estimate (see [22, Proposition 1.135]): there exists

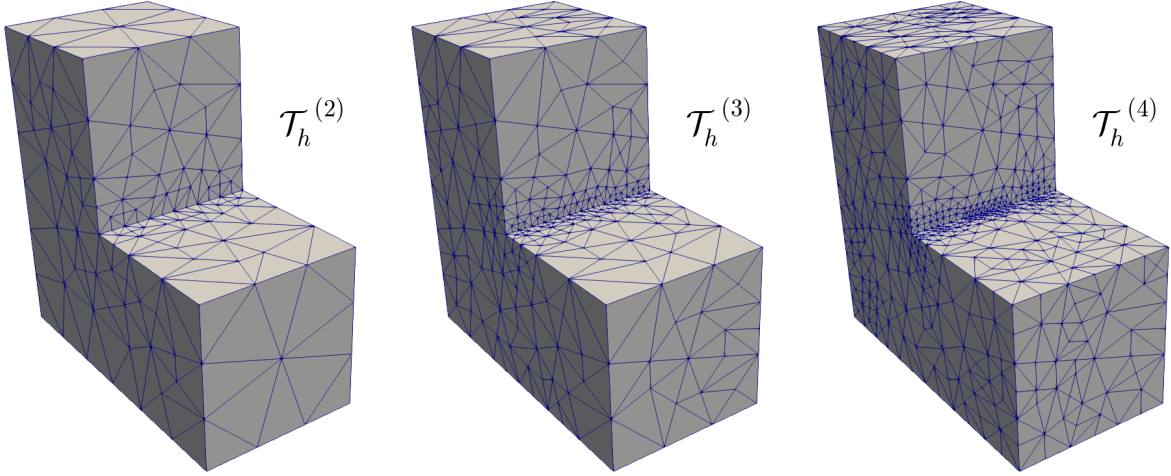


Figure 4.6: [Example 3] Three snapshots of adapted meshes according to the indicator  $\Theta$  for the AFW<sub>0</sub>-based discretization.

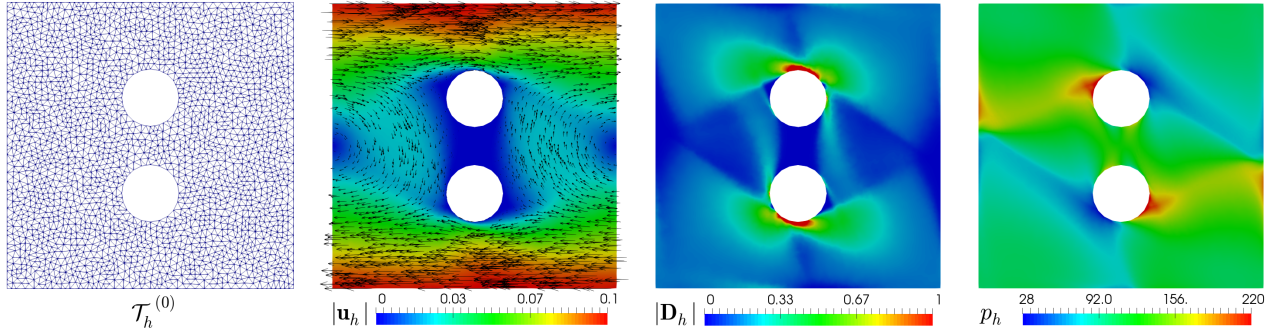


Figure 4.7: [Example 4] Initial mesh, computed magnitude of the velocity and symmetric part of the velocity gradient, and pressure field.

a positive constant  $C_0$ , independent of  $h$ , such that for  $0 \leq l \leq \ell + 1$  and  $1 \leq p \leq \infty$ , the following holds

$$\|w - \mathcal{P}_h^\ell(w)\|_{0,p;\Omega} \leq C_0 h^l \|w\|_{l,p;\Omega} \quad \forall w \in \mathbf{W}^{l,p}(\Omega). \quad (\text{A.7})$$

We stress that  $\mathcal{P}_h^\ell(w)|_K = \mathcal{P}_K^\ell(w|_K) \forall w \in \mathbf{L}^p(\Omega)$ , where  $\mathcal{P}_K^\ell : \mathbf{L}^p(K) \rightarrow \mathbf{P}_\ell(K)$  is the corresponding local orthogonal projector. In addition, denoting by  $\mathbf{P}_\ell(\Omega)$  the vector version of  $\mathbf{P}_\ell(\Omega)$  (cf. (A.5)), we let  $\mathcal{P}_h^\ell : \mathbf{L}^2(\Omega) \rightarrow \mathbf{P}_\ell(\Omega)$  be the vector version of  $\mathcal{P}_h^\ell$ .

Next, we collect some approximation proprieties of  $\Pi_h^\ell$ .

**Lemma A.1.** *Given  $p > 1$ , there exist positive constants  $C_1, C_2$ , independent of  $h$ , such that for  $0 \leq l \leq \ell$ , and for each  $K \in \mathcal{T}_h$ , there holds*

$$\|\boldsymbol{\tau} - \Pi_h^\ell(\boldsymbol{\tau})\|_{0,p;K} \leq C_1 h_K^{l+1} |\boldsymbol{\tau}|_{l+1,p;K} \quad \forall \boldsymbol{\tau} \in \mathbf{W}^{l+1,p}(K) \quad (\text{A.8})$$

and

$$\|\boldsymbol{\tau} \cdot \boldsymbol{\nu} - \Pi_h^\ell(\boldsymbol{\tau}) \cdot \boldsymbol{\nu}\|_{0,p;e} \leq C_2 h_e^{1-1/p} |\boldsymbol{\tau}|_{1,p;K} \quad \forall \boldsymbol{\tau} \in \mathbf{W}^{1,p}(K), \quad \forall e \in \mathcal{E}_h(K). \quad (\text{A.9})$$

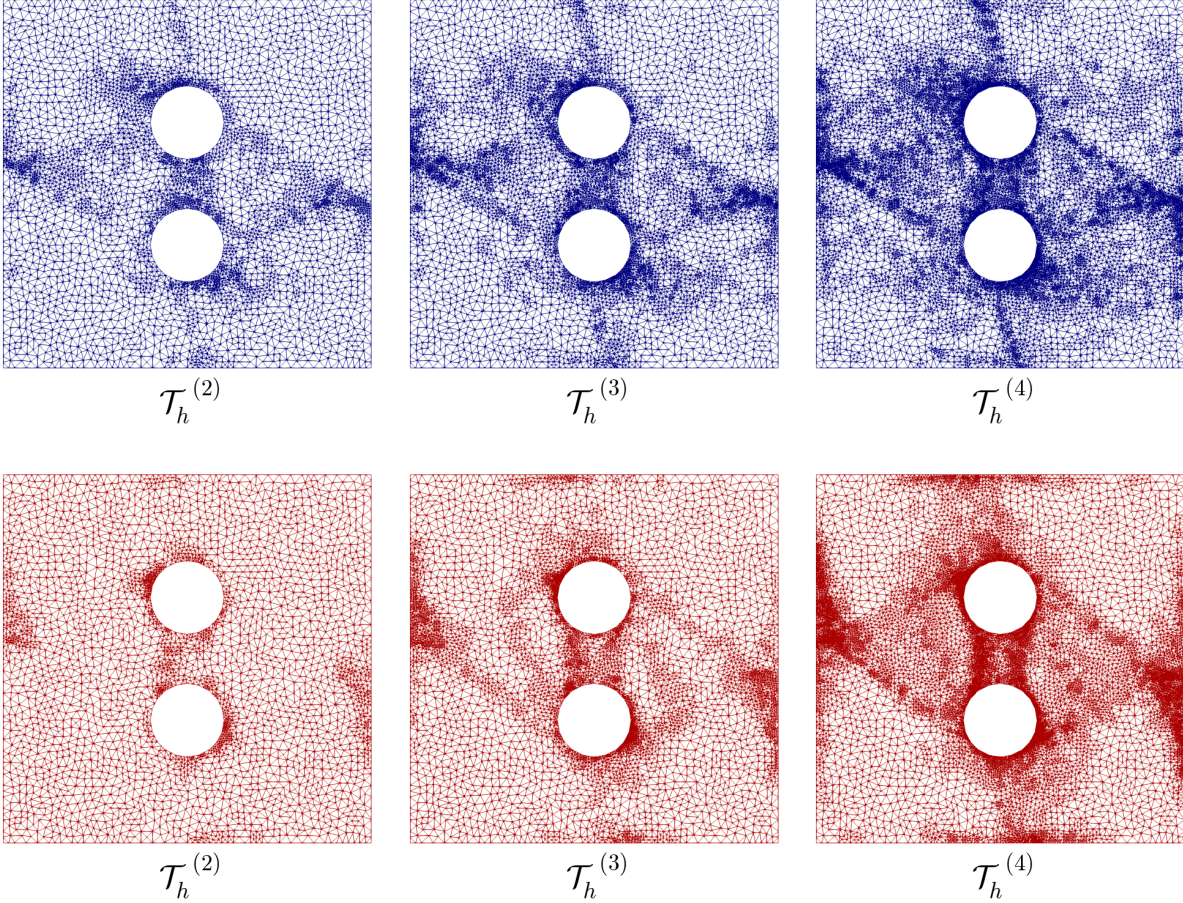


Figure 4.8: [Example 4] Three snapshots of adapted meshes according to the indicator  $\Theta$  for PEERS<sub>0</sub> and AFW<sub>0</sub>-based discretizations (top and bottom plots, respectively).

*Proof.* For the estimate (A.8) we refer to [28, Lemma 3.1], whereas the proof of (A.9) can be found in [8, Lemma 4.2].  $\square$

At this point, we emphasize that, since the Brezzi–Douglas–Marini (BDM) interpolation operator satisfies properties analogous to (A.3), (A.4), and (A.6) (cf. [7, Sections III.3]), it is also possible to prove the approximation estimates (A.8) and (A.9) in Lemma A.1 for this operator. Consequently, Lemma 3.4 can also be derived for the AFW-based approach (2.20).

Furthermore, denoting by  $\mathbb{W}_p(\Omega)$  and  $\mathbb{RT}_\ell(\Omega)$  the tensorial versions of  $\mathbf{W}_p(\Omega)$  (cf. (A.1)) and  $\mathbf{RT}_\ell(\Omega)$  (cf. (A.2)), respectively, we let  $\mathbf{\Pi}_h^\ell : \mathbb{W}_p(\Omega) \rightarrow \mathbb{RT}_\ell(\Omega)$  be the operator  $\mathbf{\Pi}_h^\ell$  acting row-wise. Then, and similarly to decomposition (2.9), for each  $\boldsymbol{\tau} \in \mathbb{W}_p(\Omega)$  there holds

$$\mathbf{\Pi}_h^\ell(\boldsymbol{\tau}) := \mathbf{\Pi}_{h,0}^\ell(\boldsymbol{\tau}) + c_0 \mathbb{I}, \quad \text{with} \quad c_0 := \frac{1}{n|\Omega|} \int_{\Omega} \text{tr} \left( \mathbf{\Pi}_h^\ell(\boldsymbol{\tau}) \right) \in \mathbb{R}$$

$$\text{and} \quad \mathbf{\Pi}_{h,0}^\ell(\boldsymbol{\tau}) := \mathbf{\Pi}_h^\ell(\boldsymbol{\tau}) - c_0 \mathbb{I} \in \mathbb{RT}_\ell(\Omega) \cap \mathbb{H}_0(\mathbf{div}_p; \Omega),$$

where  $\mathbb{H}_0(\mathbf{div}_p; \Omega) := \left\{ \boldsymbol{\tau} \in \mathbb{H}(\mathbf{div}_p; \Omega) : \int_{\Omega} \text{tr}(\boldsymbol{\tau}) = 0 \right\}$ . Additional approximation properties of  $\mathbf{\Pi}_h^\ell$  and  $\mathbf{\Pi}_{h,0}^\ell$ , particularly those involving the  $\text{div}$  and  $\mathbf{div}$  operators, can also be established using (A.6)

and (A.7), along with their tensorial counterparts for  $\mathbf{\Pi}_h^\ell$  and  $\mathcal{P}_h^\ell$ .

We now recall from [8, Lemma 4.4] a stable Helmholtz decomposition for the nonstandard Banach space  $\mathbb{H}(\mathbf{div}_p; \Omega)$ , which will be used in the forthcoming analysis for the particular case  $p = 4/3$ . More precisely, we state the following result:

**Lemma A.2.** *Given  $p \in (1, 2)$ , there exists a positive constant  $C_p$  such that for each  $\boldsymbol{\tau} \in \mathbb{H}(\mathbf{div}_p; \Omega)$  there exist  $\boldsymbol{\zeta} \in \mathbb{W}^{1,p}(\Omega)$  and  $\boldsymbol{\xi} \in \mathbf{H}^1(\Omega)$  satisfying*

$$\boldsymbol{\tau} = \boldsymbol{\zeta} + \mathbf{curl}(\boldsymbol{\xi}) \quad \text{in } \Omega \quad \text{and} \quad \|\boldsymbol{\zeta}\|_{1,p;\Omega} + \|\boldsymbol{\xi}\|_{1,\Omega} \leq C_p \|\boldsymbol{\tau}\|_{\mathbf{div}_p;\Omega}. \quad (\text{A.10})$$

On the other hand, let us define  $X_h := \{v_h \in C(\overline{\Omega}) : v_h|_K \in P_1(K) \quad \forall K \in \mathcal{T}_h\}$  and denote by  $\mathbf{X}_h$  its vector-valued counterpart. We consider the Clément interpolation operator  $\mathcal{I}_h : \mathbf{H}^1(\Omega) \rightarrow \mathbf{X}_h$  and its vector version  $\boldsymbol{\mathcal{I}}_h : \mathbf{H}^1(\Omega) \rightarrow \mathbf{X}_h$ . Some local properties of  $\mathcal{I}_h$ , and consequently of  $\boldsymbol{\mathcal{I}}_h$ , corresponding to the particular case of [22, Lemma 1.127] with  $m = 2$ ,  $p = 2$ , and  $\ell = 1$ , are established in the following lemma (cf. [19]).

**Lemma A.3.** *There exist positive constants  $C_1$  and  $C_2$ , such that for each  $v \in H^1(\Omega)$  there hold*

$$\|v - \mathcal{I}_h(v)\|_{0,K} \leq C_1 h_K \|v\|_{1,\Delta(K)} \quad \forall K \in \mathcal{T}_h$$

and

$$\|v - \boldsymbol{\mathcal{I}}_h(v)\|_{0,e} \leq C_2 h_e^{1/2} \|v\|_{1,\Delta(e)} \quad \forall K \in \mathcal{E}_h,$$

where  $\Delta(K) := \cup\{K' \in \mathcal{T}_h : K' \cap K \neq \emptyset\}$  and  $\Delta(e) := \cup\{K' \in \mathcal{T}_h : K' \cap e \neq \emptyset\}$ .

## B Preliminaries for efficiency

For the efficiency analysis of  $\Theta$  (cf. (3.1)), we proceed as in [6, 29, 26, 15, 28, 8, 13], and apply the localization technique based on bubble functions, along with inverse and discrete trace inequalities. For the former, given  $K \in \mathcal{T}_h$ , we let  $\psi_K$  be the usual element-bubble function (cf. [39, eq. (1.5)]), satisfying

$$\psi_K \in P_3(K), \quad \text{sup}(\psi_K) \subseteq K, \quad \psi_K = 0 \quad \text{on } \partial K \quad \text{and} \quad 0 \leq \psi_K \leq 1 \quad \text{in } K. \quad (\text{B.1})$$

The specific properties of  $\psi_K$  are collected in the following lemma, for whose proof we refer to [39, Lemma 3.3].

**Lemma B.1.** *Let  $\ell$  be a non-negative integer, and  $p, q \in (1, +\infty)$  conjugate to each other, that is, such that  $1/p + 1/q = 1$ , and let  $K \in \mathcal{T}_h$ . Then, there exist positive constants  $c_1, c_2$ , and  $c_3$ , independent of  $h$  and  $K$ , but depending on the shape-regularity of the triangulations (minimum angle condition) and  $\ell$ , such that for each  $u \in P_\ell(K)$  there hold*

$$c_1 \|u\|_{0,p;K} \leq \sup_{0 \neq v \in P_\ell(K)} \frac{\int_K u \psi_K v}{\|v\|_{0,q;K}} \leq \|u\|_{0,p;K}$$

and

$$c_2 h_K^{-1} \|\psi_K u\|_{0,q;K} \leq \|\nabla(\psi_K u)\|_{0,q;K} \leq c_3 h_K^{-1} \|\psi_K u\|_{0,q;K}.$$

In turn, the aforementioned inverse inequality is stated as follows (cf. [22, Lemma 1.138]).

**Lemma B.2.** *Let  $\ell, l$  and  $m$  be non-negative integers such that  $m \leq l$ , and let  $r, s \in [1, +\infty]$ , and  $K \in \mathcal{T}_h$ . Then, there exists  $c > 0$ , independent of  $h, K, r$  and  $s$ , but depending on  $\ell, l, m$  and the shape-regularity of the triangulations, such that*

$$\|v\|_{l,r;K} \leq ch_K^{m-l+n(1/r-1/s)} \|v\|_{m,s;K} \quad \forall v \in P_\ell(K). \quad (\text{B.2})$$

Finally, proceeding as in [1, Theorema 3.10], that is employing the usual scaling estimates with respect to a fixed reference element  $\hat{K}$ , and applying the trace inequality in  $W^{1,p}(\hat{K})$ , for a given  $p \in (1, +\infty)$ , one is able to establish the following discrete trace inequality.

**Lemma B.3.** *Let  $p \in (1, +\infty)$ . Then, there exists  $c > 0$ , depending only on the shape regularity of the triangulations, such that for each  $K \in \mathcal{T}_h$  and  $e \in \mathcal{E}_h(K)$ , there holds*

$$\|v\|_{0,p;e}^p \leq c \left\{ h_K^{-1} \|v\|_{0,p;K}^p + h_K^{p-1} |v|_{1,p;K}^p \right\} \quad \forall v \in W^{1,p}(K). \quad (\text{B.3})$$

## C A posteriori error analysis: the 3D case

In this appendix, we extend the results from Section 3 to the three-dimensional version of (2.21). Similarly to the previous section, given a tetrahedron  $K \in \mathcal{T}_h$ , we denote by  $\mathcal{E}_K$  the set of its faces and by  $\mathcal{E}$  the set of all faces in the triangulation  $\mathcal{T}_h$ . We then define  $\mathcal{E}_h = \mathcal{E}_h(\Omega) \cup \mathcal{E}_h(\Gamma)$ , where  $\mathcal{E}_h(\Omega) := \{e \in \mathcal{E}_h : e \subseteq \Omega\}$  and  $\mathcal{E}_h(\Gamma) := \{e \in \mathcal{E}_h : e \subseteq \Gamma\}$ . For each face  $e \in \mathcal{E}_h$ , we fix a unit normal vector  $\boldsymbol{\nu}_e$ . Given  $\boldsymbol{\tau} = (\tau_{ij})_{3 \times 3} \in \mathbb{L}^2(\Omega)$  such that  $\boldsymbol{\tau}|_K \in \mathbb{C}(K)$  for each  $K \in \mathcal{T}_h$ , we define  $\llbracket \boldsymbol{\tau} \times \boldsymbol{\nu}_e \rrbracket$  as the corresponding jump of the tangential trace across  $e$ . In other words,  $\llbracket \boldsymbol{\tau} \times \boldsymbol{\nu}_e \rrbracket := (\boldsymbol{\tau}|_K - \boldsymbol{\tau}|_{K'}) \times \boldsymbol{\nu}_e$ , where  $K$  and  $K'$  are the tetrahedra in  $\mathcal{T}_h$  sharing  $e$  as a common face and

$$\boldsymbol{\tau} \times \boldsymbol{\nu}_e := \begin{pmatrix} (\tau_{11}, \tau_{12}, \tau_{13}) \times \boldsymbol{\nu}_e \\ (\tau_{21}, \tau_{22}, \tau_{23}) \times \boldsymbol{\nu}_e \\ (\tau_{31}, \tau_{32}, \tau_{33}) \times \boldsymbol{\nu}_e \end{pmatrix}.$$

From now on, when no confusion arises, we simply write  $\boldsymbol{\nu}$  instead of  $\boldsymbol{\nu}_e$ . In the sequel we will also make use of the following differential operators

$$\mathbf{curl}(\mathbf{v}) = \nabla \times \mathbf{v} := \left( \frac{\partial v_3}{\partial x_2} - \frac{\partial v_2}{\partial x_3}, \frac{\partial v_1}{\partial x_3} - \frac{\partial v_3}{\partial x_1}, \frac{\partial v_2}{\partial x_1} - \frac{\partial v_1}{\partial x_2} \right)^t,$$

and

$$\underline{\mathbf{curl}}(\boldsymbol{\tau}) := \begin{pmatrix} \mathbf{curl}(\tau_{11}, \tau_{12}, \tau_{13})^t \\ \mathbf{curl}(\tau_{21}, \tau_{22}, \tau_{23})^t \\ \mathbf{curl}(\tau_{31}, \tau_{32}, \tau_{33})^t \end{pmatrix}.$$

In turn, we will also use the tensor version of the tangential curl operator  $\mathbf{curl}_s$ , denoted by  $\underline{\mathbf{curl}}_s$ , which is defined component-wise by  $\mathbf{curl}_s$  (see [14, Section 3] for details).

We now set for each  $K \in \mathcal{T}_h$  the local estimator

$$\begin{aligned} \Theta_{2,K}^2 &:= \|\eta(p_h, |\mathbf{D}_h|) \mathbf{D}_h - \boldsymbol{\sigma}_h^d - \rho(\mathbf{u}_h \otimes \mathbf{u}_h)^d\|_{0,K}^2 + \|\boldsymbol{\sigma}_h - \boldsymbol{\sigma}_h^t\|_{0,K}^2 \\ &+ h_K^2 \|\underline{\mathbf{curl}}(\mathbf{D}_h + \boldsymbol{\gamma}_h)\|_{0,K}^2 + \sum_{e \in \mathcal{E}_h(K) \cap \mathcal{E}(\Omega)} h_e \|\llbracket (\mathbf{D}_h + \boldsymbol{\gamma}_h) \times \boldsymbol{\nu} \rrbracket\|_{0,e}^2 \\ &+ \sum_{e \in \mathcal{E}_h(K) \cap \mathcal{E}(\Gamma)} h_e \|\underline{\mathbf{curl}}_s(\mathbf{u}_D) - (\mathbf{D}_h + \boldsymbol{\gamma}_h) \times \boldsymbol{\nu}\|_{0,e}^2, \end{aligned}$$

and the global *a posteriori* error estimator is defined as

$$\Theta = \left\{ \sum_{K \in \mathcal{T}_h} \Theta_{1,K}^{4/3} \right\}^{3/4} + \left\{ \sum_{K \in \mathcal{T}_h} \Theta_{2,K}^2 \right\}^{1/2} + \left\{ \sum_{K \in \mathcal{T}_h} \Theta_{3,K}^4 \right\}^{1/4},$$

where  $\Theta_{1,K}^{4/3}$  and  $\Theta_{3,K}^4$  are defined in (3.2) and (3.4), respectively. Accordingly, the corresponding reliability and efficiency estimates, which represent the analogues of Theorems 3.1 and 3.5, are stated as follows.

**Theorem C.1.** *Assume that  $L_\eta$  and the radii  $\delta$  and  $\delta_d$  satisfy (3.10). Then, there exist positive constants  $C_{\text{eff}}$  and  $C_{\text{rel}}$ , independent of  $h$ , such that*

$$C_{\text{eff}} \Theta + \text{h.o.t} \leq \|\bar{\mathbf{D}} - \bar{\mathbf{D}}_h\|_{\mathcal{H}} + \|p - p_h\|_{0,\Omega} \leq C_{\text{rel}} \Theta.$$

The proof of Theorem C.1 follows closely the analysis in Section 3, except for a few aspects that will be discussed below. Specifically, we first observe that the general *a posteriori* error estimate given in Lemma 3.2, as well as the upper bounds for  $\|\mathcal{R}_1\|_{\mathcal{H}'_1}$  and  $\|\mathcal{R}_3\|_{\mathcal{Q}'}$  (cf. (3.26), (3.27)), remain valid in 3D. Next, we follow [25, Theorem 3.2] to derive a 3D version of the Helmholtz decomposition for arbitrary polyhedral domains, as provided by Lemma A.2, with  $p \in [6/5, 2)$  (cf. [8, Lemma 3.4]). The corresponding discrete Helmholtz decomposition and the functional  $\mathcal{R}_2$  are then established and rewritten exactly as in (3.30) and (3.31). Furthermore, to derive the new upper bounds for  $\|\mathcal{R}_2\|_{\mathcal{H}'_2}$  (cf. Lemma 3.4), we require the 3D analogue of the integration by parts formula on the boundary given in (3.36). In fact, using the identities from [31, Chapter I, eq. (2.17), and Theorem 2.11], we deduce that in this case, the following holds

$$\langle \mathbf{curl}(\boldsymbol{\xi})\boldsymbol{\nu}, \boldsymbol{\theta} \rangle_{\Gamma} = -\langle \mathbf{curl}_s(\boldsymbol{\theta}), \boldsymbol{\xi} \rangle_{\Gamma}, \quad \forall \boldsymbol{\xi} \in \mathbb{H}^1(\Omega), \quad \forall \boldsymbol{\theta} \in \mathbf{H}^{1/2}(\Gamma).$$

In addition, the integration by parts formula on each tetrahedron  $K \in \mathcal{T}_h$ , which is used in the proof of the 3D analogues of Lemma 3.4, becomes (cf. [31, Chapter I, Theorem 2.11])

$$\int_K \mathbf{curl}(\mathbf{q}) : \boldsymbol{\xi} - \int_K \mathbf{q} : \mathbf{curl}(\boldsymbol{\xi}) = \langle \mathbf{q} \times \boldsymbol{\nu}, \boldsymbol{\xi} \rangle_{\partial K}, \quad \forall \mathbf{q} \in \mathbb{H}(\mathbf{curl}; \Omega), \quad \forall \boldsymbol{\xi} \in \mathbb{H}^1(\Omega),$$

where  $\langle \cdot, \cdot \rangle_{\partial K}$  denotes the duality pairing between  $\mathbb{H}^{-1/2}(\partial K)$  and  $\mathbb{H}^{1/2}(\partial K)$ . As usual,  $\mathbb{H}(\mathbf{curl}; \Omega)$  is the space of tensor fields in  $\mathbb{L}^2(\Omega)$  whose  $\mathbf{curl}$  belongs to  $\mathbb{L}^2(\Omega)$ . We observe that, unlike the 2D case, assuming  $\mathbf{u}_D \in \mathbf{H}^1(\Gamma)$  is not necessary for the reliability analysis, since  $\mathbf{curl}_s$  is defined in  $\mathbf{H}^{1/2}(\Gamma)$ . Nevertheless, for computational purposes, in Section 4, we assume that  $\mathbf{u}_D$  is sufficiently smooth, in which case  $\mathbf{curl}_s(\mathbf{u}_D)$  coincides with  $\nabla \mathbf{u}_D \times \boldsymbol{\nu}$ .

Finally, to prove the efficiency of  $\Theta$ , we first observe that the term defining  $\Theta_{1,K}^{4/3}$  (cf. (3.2)) and the first two terms defining  $\Theta_{2,K}^2$  (cf. (3.3)) are estimated exactly as in the 2D case, following Lemma 3.6. For the remaining terms, we establish the following lemma.

**Lemma C.2.** *There exist positive constants  $C_i$ ,  $i \in \{1, \dots, 5\}$ , all independent of  $h$ , such that*

- a)  $h_K^4 \|\nabla \mathbf{u}_h - (\mathbf{D}_h + \boldsymbol{\gamma}_h)\|_{0,4;K}^4 \leq C_1 \left\{ \|\mathbf{u} - \mathbf{u}_h\|_{0,4;K}^4 + h_K^2 \|\mathbf{D} - \mathbf{D}_h\|_{0,K}^4 + h_K^2 \|\boldsymbol{\gamma} - \boldsymbol{\gamma}_h\|_{0,K}^4 \right\} \quad \forall K \in \mathcal{T}_h,$
- b)  $h_e \|\mathbf{u}_D - \mathbf{u}_h\|_{0,4;e}^4 \leq C_2 \left\{ \|\mathbf{u} - \mathbf{u}_h\|_{0,4;K_e}^4 + h_{K_e}^2 \|\mathbf{D} - \mathbf{D}_h\|_{0,K_e}^4 + h_{K_e}^2 \|\boldsymbol{\gamma} - \boldsymbol{\gamma}_h\|_{0,K_e}^4 \right\} \quad \forall e \in \mathcal{E}_h(\Gamma),$
- c)  $h_K^2 \|\mathbf{curl}(\mathbf{D}_h + \boldsymbol{\gamma}_h)\|_{0,K}^2 \leq C_3 \left\{ \|\mathbf{D} - \mathbf{D}_h\|_{0,K}^2 + \|\boldsymbol{\gamma} - \boldsymbol{\gamma}_h\|_{0,K}^2 \right\} \quad \forall K \in \mathcal{T}_h,$

$$\text{d) } h_e \left\| \llbracket (\mathbf{D}_h + \boldsymbol{\gamma}_h) \times \boldsymbol{\nu} \rrbracket \right\|_{0,e}^2 \leq C_4 \left\{ \|\mathbf{D} - \mathbf{D}_h\|_{0,\omega_e}^2 + \|\boldsymbol{\gamma} - \boldsymbol{\gamma}_h\|_{0,\omega_e}^2 \right\} \quad \forall e \in \mathcal{E}_h(\Omega),$$

$$\text{e) } h_e \left\| \underline{\mathbf{curl}}_s(\mathbf{u}_D) - (\mathbf{D}_h + \boldsymbol{\gamma}_h) \times \boldsymbol{\nu} \right\|_{0,e}^2 \leq C_5 \left\{ \|\mathbf{D} - \mathbf{D}_h\|_{0,K_e}^2 + \|\boldsymbol{\gamma} - \boldsymbol{\gamma}_h\|_{0,K_e}^2 \right\}, \quad \forall e \in \mathcal{E}_h(\Gamma),$$

where  $K_e$  is the tetrahedron in  $\mathcal{T}_h$  having  $e$  as a face, whereas  $\omega_e$  denotes the union of the two elements in  $\mathcal{T}_h$  that share the face  $e$ .

*Proof.* For a), we refer again to [28, Lemma 3.15] by using now the local inverse inequality (B.2) with  $n = 3$ , whereas b) follows from [28, Lemma 3.16], (B.3) and the estimate in a). In addition, for the proof of c), we refer to [6, Lemma 4.3], while the proof of d) follows from [6, Lemma 4.4]. Finally, e) can be derived after a slight modification of the proof of [29, Lemma 4.15], along with the definition of  $\underline{\mathbf{curl}}_s$ .  $\square$

## References

- [1] S. AGMON, *Lectures on elliptic boundary value problems*. Van Nostrand, Princeton, NJ, (1965).
- [2] M. AINSWORTH AND J.T. ODEN, *A posteriori error estimators for the Stokes and Oseen equations*. SIAM J. Numer. Anal. 34 (1997), no. 1, 228–245.
- [3] M. AINSWORTH AND J.T. ODEN, *A Posteriori Error Estimation in Finite Element Analysis*. Pure and Applied Mathematics (New York). Wiley-Interscience [John Wiley & Sons], New York, 2000.
- [4] A. ALLENDES, E. OTAROLA, AND A.J. SALGADO, *A posteriori error estimates for the stationary Navier–Stokes equations with Dirac measures*. SIAM J. Sci. Comput. 42 (2020), no. 3, A1860–A1884.
- [5] M.S. ALNAES, J. BLECHTA, J. HAKE, A. JOHANSSON, B. KEHLET, A. LOGG, C. RICHARDSON, J. RING, M.E. ROGNES, AND G.N. WELLS, *The FEniCS project version 1.5*. Arch. Numer. Softw. 3 (2015) 9–23.
- [6] T.P. BARRIOS, G.N. GATICA, M. GONZÁLEZ, AND N. HEUER, *A residual based a posteriori error estimator for an augmented mixed finite element method in linear elasticity*. Math. Mod. and Num. Anal. 40 (2006), no. 5, 843–869.
- [7] F. BREZZI AND M. FORTIN, *Mixed and Hybrid Finite Element Methods*. Springer Series in Computational Mathematics, 15. Springer-Verlag, New York, 1991.
- [8] J. CAMAÑO, S. CAUCAO, R. OYARZÚA, AND S. VILLA-FUENTES, *A posteriori error analysis of a momentum conservative Banach spaces based mixed-FEM for the Navier–Stokes problem*. Appl. Numer. Math. 176 (2022), 134–158.
- [9] J. CAMAÑO, G.N. GATICA, R. OYARZÚA, AND R. RUIZ-BAIER, *An augmented stress-based mixed finite element method for the steady state Navier-Stokes equations with nonlinear viscosity*. Numer. Methods Partial Differential Equations 33 (2017), no. 5, 1692–1725.
- [10] C. CARSTENSEN, *A posteriori error estimate for the mixed finite element method*. Math. Comp. 66 (1997), no. 218, 465–476.

- [11] C. CARSTENSEN AND G. DOLZMANN, *A posteriori error estimates for mixed FEM in elasticity*. Numer. Math. 81 (1998), no. 2, 187–209.
- [12] S. CAUCAO, G.N. GATICA, S.R. MEDRADO, AND Y.D. SOBRAL, *Nonlinear twofold saddle point-based mixed finite element methods for a regularized  $\mu(I)$ -rheology model of granular materials*. J. Comput. Phys. 520 (2025) 113462.
- [13] S. CAUCAO, G.N. GATICA, AND J.P. ORTEGA, *A posteriori error analysis of a Banach spaces-based fully mixed FEM for double-diffusive convection in a fluid-saturated porous medium*. Comput. Geosci. 27 (2023), no. 2, 289–316.
- [14] S. CAUCAO, G.N. GATICA, AND R. OYARZÚA, *A posteriori error analysis of a fully-mixed formulation for the Navier–Stokes/Darcy coupled problem with nonlinear viscosity*. Comput. Methods Appl. Mech. Engrg. 315, (2017), 943–971.
- [15] S. CAUCAO, G.N. GATICA, R. OYARZÚA, AND F. SANDOVAL, *Residual-based a posteriori error analysis for the coupling of the Navier–Stokes and Darcy–Forchheimer equations*. ESAIM: Math. Model. and Num. Anal., 55 (2021), no. 2, 659–687.
- [16] S. CAUCAO, G.N. GATICA, AND F. SANDOVAL, *A fully-mixed finite element method for the coupling of the Navier–Stokes and Darcy–Forchheimer equations*. Numer. Methods Partial Differential Equations 37 (2021), no. 3, 2550–2587.
- [17] S. CAUCAO, D. MORA, AND R. OYARZÚA, *A priori and a posteriori error analysis of a pseudostress-based mixed formulation of the Stokes problem with varying density*. IMA J. Numer. Anal. 36 (2016), no. 2, 947–983.
- [18] S. CAUCAO, R. OYARZÚA, AND S. VILLA-FUENTES, *A posteriori error analysis of a momentum and thermal energy conservative mixed-FEM for the Boussinesq equations*. Calcolo 59 (2022), no. 4, Paper No. 45, 40 pp.
- [19] P. CLÉMENT, *Approximation by finite element functions using local regularization*. RAIRO Modélisation Mathématique et Analyse Numérique 9 (1975), 77–84.
- [20] E. CREUSÉ, M. FARHLOUL, AND L. PAQUET, *A posteriori error estimation for the dual mixed finite element method for the  $p$ -Laplacian in a polygonal domain*. Comput. Methods in Appl. Mech. and Engrg. 196 (2007), no. 25–28, 2570–2582.
- [21] C. DOMÍNGUEZ, G. N. GATICA, AND S. MEDDAHI, *A posteriori error analysis of a fully-mixed finite element method for a two-dimensional fluid-solid interaction problem*. J. Comput. Math. 33 (2015), no. 6, 606–641.
- [22] A. ERN AND J.-L. GUERMOND, *Theory and Practice of Finite Elements*. Applied Mathematical Sciences, 159. Springer-Verlag, New York, 2004.
- [23] M. FARHLOUL, S. NICAISE, AND L. PAQUET, *A priori and a posteriori error estimations for the dual mixed finite element method of the Navier–Stokes problem*. Numer. Methods Partial Differential Equations 25 (2009), no. 4, 843–869.
- [24] G.N. GATICA, *A Simple Introduction to the Mixed Finite Element Method. Theory and Applications*. SpringerBriefs in Mathematics. Springer, Cham, 2014.

- [25] G.N. GATICA, *A note on stable Helmholtz decompositions in 3D*. *Applicable Analysis*, 99, (2020), no. 7, 1110–1121.
- [26] G.N. GATICA, L.F. GATICA, AND F.A. SEQUEIRA, *A priori and a posteriori error analyses of a pseudostress-based mixed formulation for linear elasticity*. *Comp. and Math. with App.*, 71, (2016), no. 2, 585–614.
- [27] G.N. GATICA, N. HEUER, AND S. MEDDAHI, *On the numerical analysis of nonlinear twofold saddle point problems*. *IMA J. Numer. Anal.* 23 (2003), no. 2, 301–330.
- [28] G.N. GATICA, C. INZUNZA, R. RUIZ-BAIER, AND F. SANDOVAL, *A posteriori error analysis of Banach spaces-based fully-mixed finite element methods for Boussinesq-type models*. *J. of Num. Math.*, 30, (2022) no. 4, pp. 325–356.
- [29] G.N. GATICA, A. MÁRQUEZ, AND M.A. SÁNCHEZ, *Analysis of a velocity-pressure-pseudostress formulation for the stationary Stokes equations*. *Comput. Methods Appl. Mech. Engrg.* 199 (2010), 1064–1079.
- [30] G.N. GATICA, R. RUIZ-BAIER, AND G. TIERRA, *A posteriori error analysis of an augmented mixed method for the Navier-Stokes equations with nonlinear viscosity*. *Comput. Math. Appl.* 72 (2016), no. 9, 2289–2310.
- [31] V. GIRAULT AND P.A. RAVIART, *Finite Element Methods for Navier–Stokes Equations. Theory and Algorithms*. Springer Series in Computational Mathematics, 5. Springer-Verlag, Berlin, 1986.
- [32] P. JOP, Y. FORTERRE, AND O. POULIQUEN, *A constitutive law for dense granular flows*. *Nature* 441 (2008), no. 8, 727–730.
- [33] G. KANSCHAT AND D. SCHÖTZAU, *Energy norm a posteriori error estimation for divergence-free discontinuous Galerkin approximations of the Navier–Stokes equations*. *Internat. J. Numer. Methods Fluids* 57 (2008), no. 9, 1093–1113.
- [34] M. LONSING AND R. VERFÜRTH, *A posteriori error estimators for mixed finite element methods in linear elasticity*. *Numer. Math.* 97 (2004), no. 4, 757–778.
- [35] J.T. ODEN, W. WU, AND M. AINSWORTH. *An a posteriori error estimate for finite element approximations of the Navier–Stokes equations*. *Comput. Methods Appl. Mech. Engrg.* 111 (1994), no. 1-2, 185–202.
- [36] A. PLAZA AND G.F. CAREY, *Local refinement of simplicial grids based on the skeleton*. *Appl. Numer. Math.* 32 (2000), no. 2, 195–218.
- [37] S. REPIN, S. SAUTER, AND A. SMOLIANSKI, *Two-sided a posteriori error estimates for mixed formulations of elliptic problems*. *SIAM J. Numer. Anal.* 45 (2007), no. 3, 928–945.
- [38] R. VERFÜRTH, *A posteriori error estimates for non-linear problems. Finite element discretizations of elliptic equations*. *Math. Comp.* 62 (1994), no. 206, 445–475.
- [39] R. VERFÜRTH, *A Review of Posteriori Error Estimation & Adaptive Mesh-Refinement Techniques*. Wiley, (1996).
- [40] R. VERFÜRTH, *A posteriori error estimators and adaptive mesh-refinement techniques for the Navier–Stokes equations*. *Incompressible computational fluid dynamics: Trends and advances*, 447–476, Cambridge Univ. Press, Cambridge, 2008.

# Centro de Investigación en Ingeniería Matemática (CI<sup>2</sup>MA)

## PRE-PUBLICACIONES 2024 - 2025

- 2024-25 SERGIO CARRASCO, SERGIO CAUCAO, GABRIEL N. GATICA: *A twofold perturbed saddle point-based fully mixed finite element method for the coupled Brinkman Forchheimer Darcy problem*
- 2024-26 JUAN BARAJAS-CALONGE, RAIMUND BÜRGER, PEP MULET, LUIS M. VILLADA: *Invariant-region-preserving central WENO schemes for one-dimensional multispecies kinematic flow models*
- 2024-27 RAIMUND BÜRGER, CLAUDIO MUÑOZ, SEBASTIÁN TAPIA: *Interaction of jamitons in second-order macroscopic traffic models*
- 2025-01 BOUMEDIENE CHENTOUF, SABEUR MANSOURI, MAURICIO SEPÚLVEDA, RODRIGO VÉJAR: *Theoretical and numerical results for the exponential stability of the rotating disk-beam system with a boundary infinite memory of type angular velocity*
- 2025-02 JULIO ARACENA, ARTURO ZAPATA-CORTÉS: *Hamiltonian dynamics of boolean networks*
- 2025-03 RAIMUND BÜRGER, ANDRÉS GUERRA, CARLOS A. VEGA: *An entropy stable and well-balanced scheme for an augmented blood flow model with variable geometrical and mechanical properties*
- 2025-04 ALONSO BUSTOS, SERGIO CAUCAO, GABRIEL N. GATICA, BENJAMÍN VENEGAS: *New fully mixed finite element methods for the coupled convective Brinkman-Forchheimer and nonlinear transport equations*
- 2025-05 FAHIM ASLAM, ZAYD HAJJEJ, JIANGHAO HAO, MAURICIO SEPÚLVEDA: *Global Existence and Asymptotic Profile of an Infinite Memory Logarithmic Wave Equation with Fractional Derivative and Strong Damping*
- 2025-06 JESSIKA CAMAÑO, RICARDO OYARZÚA, KATHERINE ROJO: *A momentum and mass conservative pseudostress-based mixed finite element method for the Stokes problem*
- 2025-07 ANÍBAL CORONEL, FERNANDO HUANCAS, MAURICIO SEPÚLVEDA: *Theoretical and numerical approaches of reaction term identification in a SIS reaction diffusion system*
- 2025-08 ISAAC BERMUDEZ, GABRIEL N. GATICA, JUAN P. SILVA: *A new Banach spaces-based mixed finite element method for the coupled Navier–Stokes and Darcy equations*
- 2025-09 SERGIO CAUCAO, GABRIEL N. GATICA, SAULO MEDRADO, YURI D. SOBRAL: *A posteriori error analysis of mixed finite element methods for a regularized  $\mu(I)$ -rheology model of granular materials*

Para obtener copias de las Pre-Publicaciones, escribir o llamar a: DIRECTOR, CENTRO DE INVESTIGACIÓN EN INGENIERÍA MATEMÁTICA, UNIVERSIDAD DE CONCEPCIÓN, CASILLA 160-C, CONCEPCIÓN, CHILE, TEL.: 41-2661324, o bien, visitar la página web del centro: <http://www.ci2ma.udec.cl>



**CENTRO DE INVESTIGACIÓN EN  
INGENIERÍA MATEMÁTICA (CI<sup>2</sup>MA)  
Universidad de Concepción**



Casilla 160-C, Concepción, Chile  
Tel.: 56-41-2661324/2661554/2661316  
<http://www.ci2ma.udec.cl>



---